Research Square

Preprints are preliminary reports that have not undergone peer review.
They should not be considered conclusive, used to inform clinical practice,
or referenced by the media as validated information.

Complement C1q drives skeletal muscle wasting in pancreatic cancer

Andrew Judge

arjudge@phhp.ufl.edu

Department of Physical Therapy, College of Public Health and Health Professions, University of Florida
https://orcid.org/0000-0002-4488-291X

Jeremy Ducharme
University of Florida https://orcid.org/0000-0003-1653-8721

Martin Schonk
University of Florida https://orcid.org/0000-0002-0035-8219

Brittney Poole
University of Florida

Nour Al-Zaeed
University of Florida

Sarah Duckett
University of Florida

Rebecca Vogt
University of Florida

Talya Binienda
University of Florida

Margaret Park
H. Lee Moffitt Cancer Center and Research Institute

Jennifer Permuth
H. Lee Moffitt Cancer Center and Research Institute, https://orcid.org/0000-0002-4726-9264

Daniel Delitto
Stanford University https://orcid.org/0000-0002-2838-5841

Carl Atkinson
Northwestern University

Sarah Judge
University of Florida https://orcid.org/0000-0002-3974-0247

Article

Keywords: cancer cachexia, muscle, tumor, atrophy, inflammation, fibrosis

Posted Date: November 9th, 2026

DOI: https://doi.org/10.21203/rs.3.rs-11516792/v1

License: This work is licensed under a Creative Commons Attribution 4.0 International License.
Read Full License

Additional Declarations: There is **NO** Competing Interest.

Complement C1q drives skeletal muscle wasting in pancreatic cancer

Jeremy B. Ducharme[1], Martin M. Schonk[1,2], Brittney R. Poole[1,2], Nour M. Al-Zaeed[1], Sarah M. Duckett[1], Rebecca A. Vogt[1], Talya Binienda[1], Margaret A. Park[3], Jennifer B. Permuth[3], Daniel J. Delitto[4], Carl Atkinson[5], Sarah M. Judge[1,6,7], Andrew R. Judge[1,6,7*]

[1] Department of Physical Therapy, University of Florida, Gainesville, FL, USA.
[2] Department of Physiology & Aging, University of Florida, Gainesville, FL, USA.
[3] Department of GI Oncology, H. Lee Moffitt Cancer Center & Research Institute, Tampa, FL, USA.
[4] Department of Surgery, Stanford University School of Medicine, Stanford, CA, USA.
[5] Department of Surgery, Feinberg School of Medicine, Northwestern University, Chicago, IL, USA.
[6] Myology Institute, University of Florida, Gainesville, FL, USA.
[7] University of Florida Health Cancer Institute, Gainesville, FL, USA.

***Correspondence to:**
Andrew R. Judge, Ph.D.
Department of Physical Therapy
University of Florida
Gainesville, FL 32610
P: +1 (352) 273-9220
E: arjudge@phhp.ufl.edu

ABSTRACT
Cancer cachexia, defined by involuntary skeletal muscle loss, affects ~70% of pancreatic ductal adenocarcinoma (PDAC) patients at diagnosis and independently worsens survival. Here, we identify complement component 1q (C1q) as a driver of PDAC-induced muscle wasting, with coordinated effects across muscle, tumor, and systemic inflammatory compartments. In cachectic PDAC patient muscle, C1q partially co-deposits with IgM, and C1q mRNA correlates with reduced muscle radiation attenuation, a CT-derived measure of muscle quality. In PDAC tumors, C1q protein correlates with immunosuppressive programs and independently predicts poor survival. These findings are recapitulated in orthotopic KPC mice, where C1q mRNA is upregulated in respiratory muscle before cachexia onset, and C1q deposits in tumors and co-deposits with IgM in muscles of cachectic mice. *C1qa* deletion reduced systemic inflammatory mediators, blocked muscle atrophy, and improved activity and grip strength in KPC mice, while attenuating immune cell infiltration and extracellular matrix remodeling in respiratory muscle. Host *C1qa* deletion also suppressed angiogenic and immunosuppressive programs in KPC tumors, while increasing intratumoral $CD8^+$ T cell density and Granzyme B production. These findings position C1q as a driver of cancer-induced muscle wasting and tumor immunosuppression, supporting C1q inhibition as a potential therapeutic strategy targeting pathological features of poor-prognosis PDAC.

KEYWORDS
cancer cachexia; muscle; tumor; atrophy; inflammation; fibrosis

INTRODUCTION

Cachexia is a condition of involuntary body weight loss due to the loss of skeletal muscle, with or without fat loss[1]. It is estimated to affect up to 40% of people with cancer at the time of diagnosis but is much higher in certain cancers such as pancreatic ductal adenocarcinoma (PDAC), with ~70% of people diagnosed with PDAC presenting with cachexia[1]. Cancer cachexia worsens quality of life by restricting activities of daily living, limits eligibility for, and tolerance of, cancer therapies, and independently predicts poor survival[2–4]. Muscle wasting in PDAC is systemic, often begins before clinical diagnosis, and currently has no approved treatment. However, the effects of PDAC on muscle extend beyond atrophy alone and include immune cell infiltration, impaired regeneration, and fibrotic remodeling of the extracellular matrix[5–8], outcomes which may be interconnected[5,8–12]. Indeed, in the pre-clinical orthotopic KPC model of PDAC cachexia, in which cancer cells isolated from the tumors of the Kras; p53; Cre (KPC) mouse are injected into the pancreas of mice, we recently demonstrated that increased immune cell presence in skeletal muscle precedes atrophy and fibrotic remodeling, implicating persistent local inflammation as a potential driving mechanism[10]. However, the upstream signals that initiate and sustain the accumulation of immune populations in skeletal muscle of people and mice with PDAC remain largely unknown.

To begin to address this knowledge gap, we previously conducted an unbiased proteomic profiling of skeletal muscle from cachectic people with PDAC, and non-cancer controls, which identified an upregulated enrichment of complement pathway proteins[5]. The complement system is a central regulator of innate immune recruitment and inflammatory amplification, and its chronic dysregulation has been shown to cause tissue injury across various inflammatory conditions[13–15]. We subsequently showed that KPC mice deficient in complement component 3 (C3), the central component of the complement system, had attenuated immune cell infiltration into muscle, and attenuated muscle atrophy and fibrosis relative to wild type (WT) KPC mice, implicating complement activation in PDAC-induced muscle pathologies[5]. However, because C3 is a central convergent point for all three complement activation pathways – the classical, lectin, and alternative, the initiating complement pathway(s) in PDAC-induced muscle pathologies remained undefined. The classical complement pathway was the first complement pathway discovered and the most widely studied[16]. It is initiated when the C1 complex, which includes the recognition protein C1q, a multimeric molecule composed of C1q A, B, and C chains, together with the associated proteases C1r and C1s, engages antibodies or damage-associated ligands[13]. This engagement releases C1r and C1s which drives downstream complement activation and immune cell recruitment, and has been demonstrated in mouse models of muscular dystrophy and age-associated muscle pathology to cause fibrotic remodeling of skeletal muscle[17,18]. C1q is also elevated in the tumor microenvironment across multiple cancer types, where it has been linked to immunosuppression and adverse clinical outcomes[19–21]. Despite these findings, the role of C1q in cancer cachexia remained unknown.

Here, we show that C1q deposition is increased in skeletal muscle from cachectic mice and people with PDAC. In people with PDAC, skeletal muscle C1q expression is associated with muscle collagen content, and reduced CT-derived muscle attenuation, a measure of muscle quality that reflects replacement of skeletal muscle by adipose and/or fibrotic tissue. Moreover, tumor levels of C1q in PDAC patients are associated with stromal enrichment and immunosuppressive programs and independently predict poor survival. In the orthotopic KPC model, skeletal muscles from WT, but not *C1qa* knockout (*C1qa*$^{-/-}$) mice, showed significant immune cell infiltration, muscle atrophy and fibrotic remodeling. Moreover, KPC tumors from *C1qa*$^{-/-}$ mice exhibited transcriptional repression of programs involved in extracellular matrix remodeling, angiogenesis, and immunosuppression compared to tumors harvested from WT mice, and transcriptional upregulation of cytotoxic lymphocyte programs, all of which have been associated with improved outcomes in PDAC[22–29]. Collectively, these findings demonstrate that C1q is required for PDAC-induced cachexia, potentially acting through coordinated effects in skeletal muscle and the tumor microenvironment, thereby identifying C1q as a potential therapeutic target in pancreatic cancer cachexia.

RESULTS

Increased C1q-IgM deposition in skeletal muscle from cachectic people with PDAC

To determine the extent to which activation of the classical complement pathway occurs in skeletal muscle of patients with PDAC cachexia, we assessed deposition of IgM and C1q, a canonical initiator and pattern-recognition component of the C1 complex, respectively. Immunofluorescence staining was performed on rectus abdominis cryosections obtained at the time of tumor resection surgery from treatment-naïve people with PDAC cachexia, defined as >5% involuntary body weight loss during the 6 months preceding PDAC diagnosis[2], compared with weight-stable PDAC patients. Both IgM and C1q deposition were significantly elevated in skeletal muscle from cachectic relative to weight-stable PDAC patients (Fig. 1A-C). Moreover, regions of C1q and IgM colocalization were observed in cachectic muscle (Fig. 1D-E), consistent with antibody-mediated engagement of the C1 complex, an initiating step in classical pathway activation. Given the established role of C1q in mediating collagen deposition in other muscle pathologies[17,18], coupled with our previous findings of increased collagen deposition in skeletal muscle from cachectic PDAC patients[6,10], we performed Masson's trichrome staining on PDAC muscle sections (Fig. 1F) and found that collagen and C1q deposition positively correlated in muscle (Fig. 1G), suggesting that C1q may contribute to the increased fibrotic remodeling of cachectic muscle (Fig. 1H). In further support of C1q associating with the pathological remodeling of skeletal muscle in PDAC patients, we examined the relationship between the mRNA level of C1 complex components in skeletal muscle biopsies with CT-defined measures of muscle quantity and quality from the same patients, via extraction of data from our previously published datasets[6,30]. *C1QA*, *C1QB*, and *C1QC*, which encode the C1q recognition component of the C1 complex, and *C1R* and *C1S*, which encode the associated serine proteases that enable downstream signaling, each showed significant inverse correlations with CT-derived skeletal muscle attenuation (SMA), a metric of muscle compositional quality reflecting replacement of skeletal muscle by adipose and/or fibrotic tissue (Fig. 1I). An inverse correlation with CT-derived skeletal muscle index (SMI), an indicator of muscle size, was significant for *C1QA* ($r = -0.469$, $p = 0.0425$) but not for the remaining subunits (Fig. S1).

Tumor C1q protein expression independently predicts poor survival in people with PDAC

Having established the presence of C1q in skeletal muscle in human PDAC cachexia, and in light of prior reports of its expression in PDAC tumors[20], we next examined the prognostic relevance of PDAC tumor C1q expression. Using published PDAC tumor proteomic data from the Clinical Proteomic Tumor Analysis Consortium (CPTAC)-PDAC cohort[31], we performed a genome-wide screen of 9,324 proteins and identified 109 proteins with significant positive co-expression with each of the three C1q subunits (Pearson $r \geq 0.40$; $q < 0.05$; Fig. 2A; Table S1). The complement cascade represented one of the largest protein clusters and included C1s, C1r, C2, C3, C4a/b, C6, C8a/b, and C9, consistent with classical complement signaling and downstream complement deposition in the PDAC tumor microenvironment. The remaining proteins were distributed across five additional pathways including, coagulation and acute phase response (PROS1, FGB, LBP, APOE), extracellular matrix remodeling and epithelial to mesenchymal transition (FN1, PLOD1, COL1A2, LOXL2/3, TGFB1, POSTN, ACTIVIN A), angiogenesis and matricellular signaling (VEGFC, IGFBP4, TIMP3, CCN4), hypoxia and glycolytic metabolism (GBE1, P4HA1, ATG7), and innate immune signaling (CCL20, CD14, SPP1, VSIG4), each of which are tumor programs previously shown to correlate with poor survival in PDAC[24–29]. Consistent with these findings, patients with high tumor C1q protein levels had significantly shorter overall survival than those with low C1q levels (Fig. 2B). Univariable Cox regression further demonstrated that increasing C1q protein abundance was associated with a 34-46% increase in mortality risk across all three subunits (Table S2). Notably, C1q retained independent prognostic associations in multivariable Cox regression after adjusting for pathological stage, age, sex, and histologic grade (Table S2).

Upregulation of the C1 complex signature in human PDAC cachexia is recapitulated in the preclinical KPC model of PDAC cachexia and marks an early event preceding skeletal muscle wasting

To determine the extent to which the C1 complex signature observed in skeletal muscle of cachectic people living with PDAC is recapitulated in the pre-clinical KPC mouse model of PDAC, we first measured C1q and IgM protein deposition in diaphragm muscles from KPC tumor-bearing and cancer-free Sham mice. The diaphragm was selected for study because its transcriptomic and histological responses to KPC tumors

recapitulate human PDAC muscle pathology[32]. C1q and IgM deposition were significantly elevated in the diaphragm muscles of KPC tumor-bearing mice relative to Sham mice, and positively correlated with body weight loss, with regions of C1q-IgM colocalization in muscle of cachectic mice consistent with antibody-mediated engagement of the C1 complex (Fig. 3A-G). C1q and IgM deposition, including regions of colocalization, were also significantly elevated in tibialis anterior (TA) muscles of KPC mice relative to Sham mice, but to a lesser extent than in the diaphragm, demonstrating that this pattern of deposition in PDAC cachexia extends to a representative locomotor muscle (Fig. S2). We next leveraged our previously published diaphragm RNA-seq time course dataset in the KPC model to identify the timeline of changes of genes encoding C1 complex proteins[10]. We found that *C1qa*, *C1qb*, *C1qc*, *C1ra*, and *C1s1* were each significantly upregulated in diaphragm muscles of KPC mice prior to cachexia onset and remained elevated throughout cachexia development and progression (Fig. 3H). Moreover, and consistent with human PDAC tumors[20,33], C1q protein was also detected within KPC tumors, with deposition density positively correlating with body weight loss (Fig. 3I-J). Together, these findings show that the KPC mouse model of PDAC cachexia recapitulates key features of C1q biology observed in human PDAC cachexia, thereby supporting the further utilization of this model in mechanistic experiments to test the role of C1q in PDAC cachexia.

C1qa deletion preserves locomotor activity, grip strength, and skeletal and cardiac muscle in KPC mice

To test the role of C1q in PDAC cachexia, murine KPC pancreatic cancer cells were orthotopically injected into C57BL/6 wild type (WT) mice and *C1qa*$^{-/-}$ mice, which lack the C1q protein complex. Body weight and food intake were monitored, and, prior to tissue collection, voluntary locomotor activity and grip strength were assessed. Body weight, food intake, voluntary activity, grip strength, and tissue-level outcomes did not differ between genotypes in Sham mice (Fig. 4A-K), consistent with previous studies showing that *C1qa*$^{-/-}$ mice on a C57BL/6 background are indistinguishable from WT C57BL/6 mice under basal conditions[34]. Body weight declined progressively in both WT and *C1qa*$^{-/-}$ KPC mice (Fig. 4A). Cumulative food intake was significantly reduced in both WT KPC (-28%) and *C1qa*$^{-/-}$ KPC mice (-14%) relative to their respective non-cancer genetic controls (Sham), with a trend toward partial attenuation in *C1qa*$^{-/-}$ KPC mice relative to WT KPC ($p = 0.0825$; Fig. 4B). Voluntary locomotor activity was significantly reduced in WT KPC mice (total distance: -70%, time active: -62%) compared to WT Sham mice, but not in *C1qa*$^{-/-}$ KPC mice compared to *C1qa*$^{-/-}$ Sham mice (Fig. 4C). Maximal forelimb grip strength was reduced in both WT KPC (-24%) and *C1qa*$^{-/-}$ KPC (-12%) mice relative to their genetic Sham controls; however, grip strength was significantly higher in *C1qa*$^{-/-}$ KPC mice compared with WT KPC mice (Fig. 4D). Muscle mass was significantly reduced in WT KPC mice compared to WT Sham across locomotor (tibialis anterior -24%; gastrocnemius -17%; soleus -24%) and cardiac (-16%) muscles, but not in *C1qa*$^{-/-}$ KPC mice compared to *C1qa*$^{-/-}$ Sham (Fig. 4E-F). No differences between genotypes were observed for fat, spleen, or tumor weights (Fig. 4G). Consistent with changes in muscle mass, KPC tumors significantly reduced myofiber cross-sectional area in limb (tibialis anterior -28%), respiratory (diaphragm -31%), chewing (masseter -38%), and swallowing (digastric -34%) muscles from WT, but not *C1qa*$^{-/-}$, mice (Fig. 4H-K). *C1qa* mRNA levels were significantly increased in the tibialis anterior and diaphragm muscles of WT KPC mice compared to WT controls and undetectable in the muscles of *C1qa*$^{-/-}$ mice, with the magnitude of increase much higher in the diaphragm (>100-fold) than the tibialis anterior (~6-fold; Fig. 4L). Although *C1qa* mRNA was detected in tumors from WT mice, it was absent in tumors from *C1qa*$^{-/-}$ mice. Since both genotypes were inoculated with KPC cells that are wild type for *C1qa* this indicates that *C1qa* mRNA in WT KPC tumors is derived from host cells and not KPC cancer cells. Consistent with this, analysis of published human PDAC single-cell RNA-sequencing data demonstrated that *C1QA* expression is predominantly found in macrophages and is not detected in malignant cells (Fig. S3)[35–37]. Overall, the preservation of voluntary activity, grip strength, muscle mass, and myofiber size across functionally and anatomically distinct muscle groups establishes C1q as a central mediator required for PDAC-induced skeletal muscle wasting and functional decline.

C1qa is required for normal complement C3 deposition in diaphragm of KPC mice

To determine the extent to which complement C3 deposition, which we recently showed occurs in skeletal muscle of mice and people with PDAC[5], is dependent on *C1qa*, we measured C3 deposition in diaphragm muscles of WT and *C1qa*$^{-/-}$ Sham and KPC mice. As expected, we found that C3 deposition was significantly elevated in diaphragm muscles from WT KPC mice relative to WT controls. However, this was significantly attenuated, by 54%, in *C1qa*$^{-/-}$ KPC mice (Fig. S4A-B), indicating that *C1qa* is required for a substantial proportion of C3 deposition in the diaphragm in response to pancreatic cancer. However, since C3 deposition remained elevated in *C1qa*$^{-/-}$ KPC mice compared to *C1qa*$^{-/-}$ Sham mice, this suggests that *C1qa*-independent complement pathways may also be activated.

***C1qa*-dependent transcriptional reprogramming in the diaphragm of KPC mice**

To identify the transcriptional programs through which *C1qa* mediates KPC-induced diaphragm wasting, we performed bulk RNA-seq on diaphragm muscles from Sham, WT KPC, and *C1qa*$^{-/-}$ KPC mice. In diaphragms from WT KPC mice, we identified 3,291 differentially expressed genes (DEGs) relative to WT Sham mice ($q < 0.05$, log2FC >1), including 1,786 upregulated genes and 1,503 downregulated genes; Fig. 5A; Table S3). Of these DEGs in WT KPC mice, only 18% were similarly upregulated (323 of 1,786) and 11% similarly downregulated (167 of 1,503) in *C1qa*$^{-/-}$ KPC mice, indicating that the other DEGs are *C1qa*-dependent. *C1qa*-dependent genes upregulated in the diaphragm in response to KPC tumors were enriched for pathways associated with inflammatory response, innate immune activation, neutrophil degranulation and chemotaxis, complement and coagulation cascades, acute-phase response, and apoptotic processes (Fig. 5B-C). *C1qa*-dependent genes downregulated in the diaphragm in response to KPC tumors were enriched for pathways of oxidative phosphorylation, mitochondrial translation and organization, TCA cycle, muscle contraction, sarcomere organization, and skeletal muscle tissue development (Fig. 5B,D). While these analyses identified broad *C1qa*-dependent transcriptional programs, we next focused on genes whose KPC-induced expression changes were substantially attenuated in *C1qa*$^{-/-}$ KPC mice relative to WT KPC mice ($q < 0.10$, ≥50% fold-change attenuation). This identified 60 genes downregulated by KPC tumors and rescued by *C1qa* deletion, which annotated to pathways of microtubule cytoskeleton organization (*Dst*, *Obsl1*, *Map4*), cytoskeletal organization in muscle cells (*Ank2*, *Myh7*, *Myom3*, *Obscn*), and skeletal muscle tissue development (*Svil*, *Pax7*, *Plec*) (Fig. 5E), and 101 genes upregulated by KPC tumors and rescued by *C1qa* deletion, which annotated to pathways of inflammatory response (*Hmga1*, *Hmgb2*, *Il1r2*, *Il18rap*), apoptotic process (*Ddit4*, *Pmaip1*, *Srgn*), neutrophil chemotaxis (*Fpr1*, *Pf4*, *S100a9*, *Trem1*), and neutrophil degranulation (*Clec4d*, *Gliprl*, *Gmfg*) (Fig. 5F).

***C1qa* mediates KPC-induced immune cell infiltration and fibrotic remodeling of the diaphragm**

Having identified *C1qa*-dependent upregulation of inflammatory programs in diaphragm muscles of KPC mice, we extracted canonical immune cell gene markers to infer immune populations increased in KPC mice in a *C1qa*-dependent manner. This revealed induction of neutrophil (*Fpr1*, *S100a8*) and macrophage (*Cd68*) markers, including macrophage markers for resident (*Lyve1*) and recruited (*Cd11b*) subsets, and M1-like (*Cd38*, *Cd80*, *Cd86*, *Marco*) and M2-like (*Arg1*, *Cd163*, *Mrc1*, *Ms4a4a*, *Trem2*) polarization states, in diaphragms of WT KPC mice, all of which were attenuated by *C1qa* deletion (Fig. 6A-B). These transcriptional patterns were supported by immunofluorescence analysis, showing elevated Ly6G^{+} neutrophil and CD68^{+} macrophage accumulation in diaphragms of WT KPC mice, both of which were attenuated in *C1qa*$^{-/-}$ KPC mice (Fig. 6C-F).

Given the established role of C1q in promoting collagen deposition in other muscle pathologies[17,18], the positive correlation between C1q and fibrosis in PDAC patients we found here (Fig. 1G), and the established link between local inflammation and fibrotic remodeling of tissue[10], we next questioned whether the development of fibrosis in response to KPC tumors is dependent on *C1qa* by staining diaphragm sections with Picrosirius Red to detect and quantify collagen. Collagen content was significantly elevated in diaphragms of WT KPC mice which was prevented by *C1qa* deletion (Fig. 7A-B). Moreover, although the extracellular matrix, quantified by wheat germ agglutinin (WGA) staining, was significantly expanded in both WT KPC mice and *C1qa*$^{-/-}$ KPC mice (Fig. 7C-D), there was a trend toward partial attenuation in *C1qa*$^{-/-}$ KPC mice relative to WT KPC ($p = 0.0816$). These histological findings are further supported by

extraction of genes from the diaphragm RNA-seq dataset related to ECM remodeling, which reveal that the upregulation of genes involved in ECM structure, ECM proteases, adhesion signaling, and matricellular and ECM regulatory factors were increased in WT, but not *C1qa*$^{-/-}$, KPC mice (Fig. 7E-F).

Loss of *C1qa* partially attenuates KPC-induced inflammatory and atrophy-associated transcriptional programs in limb skeletal muscle

To further determine the extent to which *C1qa* deletion attenuates KPC-induced transcriptional remodeling in skeletal muscle beyond the diaphragm, bulk RNA seq was performed on tibialis anterior (TA) muscles from WT Sham, WT KPC, *C1qa*$^{-/-}$ Sham, and *C1qa*$^{-/-}$ KPC mice (Fig. S5). This identified 4,439 DEGs in WT KPC mice relative to WT Sham ($q < 0.01$, log2FC >1), including 2,057 upregulated and 2,382 downregulated genes (Fig. S5A; Table S4). Notably, 39% of genes upregulated in WT KPC mice (801 of 2,057) and 53% of genes downregulated in WT KPC mice (1,258 of 2,382) were no longer differentially expressed following *C1qa* deletion, indicating partial normalization of the TA muscle transcriptome. Pathway enrichment analysis revealed that genes upregulated in WT, but not *C1qa*$^{-/-}$, KPC mice annotated to pathways associated with inflammation and stress, including cytokine signaling, TGF-β and IL-1 signaling, and platelet activation, whereas genes downregulated in WT, but not *C1qa*$^{-/-}$, KPC mice were enriched for pathways involved in muscle contraction, sarcomere organization, and mitochondrial translation (Fig. S5B). The preservation of TA muscle mass and myofiber cross-sectional area (Fig. 4F,H), together with the attenuation of inflammatory and atrophy-associated transcriptional programs in KPC mice lacking *C1qa*, further support a key role for C1q in mediating PDAC-induced muscle loss.

***C1qa* contributes to systemic pro-cachectic inflammatory signaling in KPC mice**

To assess whether the muscle-sparing effects of *C1qa* deletion are associated with systemic changes in circulating inflammatory mediators, we profiled serum cytokines in WT KPC, *C1qa*$^{-/-}$ KPC, and their respective Sham controls (Fig. S6; Table S5). Several pro-inflammatory mediators, including CCL2, TNF-α, IL-1β, and IL-2, were significantly elevated in WT KPC mice, but not in *C1qa*$^{-/-}$ KPC mice, relative to their respective Sham controls. CCL2, a chemokine implicated in cachexia[38–40], was also significantly lower in *C1qa*$^{-/-}$ KPC mice than in WT KPC mice. *C1qa* deletion also attenuated the KPC-induced increase in circulating levels of Activin A, a TGF-β family member whose circulating levels correlate with cachexia severity and mortality in PDAC[41]. Similarly, GDF-15, a stress-induced cytokine that suppresses appetite and drives weight loss in cancer[42], was significantly elevated in WT KPC mice, with only a trend toward elevation in *C1qa*$^{-/-}$ KPC mice ($p = 0.107$). In contrast, IL-6 and IL-10 were similarly elevated in both KPC tumor-bearing groups, independent of genotype. Together, these data suggest that *C1qa* partially contributes to the systemic inflammatory signaling associated with PDAC cachexia.

***C1qa* deletion reprograms the KPC tumor microenvironment toward cytotoxic immunity and suppresses pro-tumor transcriptional programs**

Given that C1q is deposited within KPC tumors (Fig. 3I), consistent with observations in human PDAC[20,33], we questioned the extent to which *C1qa* deletion remodels the tumor transcriptome. To do this we performed bulk RNA-seq on KPC tumors from WT and *C1qa*$^{-/-}$ mice, which revealed 4,162 DEGs ($q < 0.05$, FC >1.2) including 2,546 upregulated and 1,616 downregulated genes in KPC tumors with *C1qa* deletion (Fig. 8A; Table S6). Upregulated genes were enriched for epithelial differentiation programs, including cytokeratins (*Krt13*, *Krt15*, *Krt17*, *Krt23*), the epithelial marker *Tacstd2*, and transcription factors associated with epithelial identity (*Trp63*, *Tcf21*, *Ehf*), suggestive of a more differentiated phenotype. In parallel, cytokine signaling pathways were also upregulated, with increased expression of *Il7*, *Il6st*, *Lifr*, *Jak1*, *Stat5a/b*, and multiple interleukin receptor subunits (*Il1r1*, *Il1r2*, *Il2rb*, *Il5ra*, *Il31ra*) (Fig. 8A-B). This was accompanied by increased expression of genes associated with cytotoxic immune programs, including natural killer and CD8$^+$ T cell–related markers (*Klrd1*, *Klrk1*, *Cd160*, *Cd8a*, *Ncr1*) and cytotoxic effector molecules (*Gzma*, *Gzmb*, *Ifng*, *Nkg7*, *Prf1*) (Fig. 8C). Consistent with this transcriptional profile, immunohistochemical staining confirmed increased CD8$^+$ T cell and Granzyme B expression in KPC tumors from *C1qa*$^{-/-}$ mice compared to KPC tumors from WT mice (Fig. 8D-E), supporting the presence

of a more cytotoxic immune microenvironment, a feature previously associated with improved survival in people with PDAC[22,23]. Genes downregulated in tumors from *C1qa*$^{-/-}$ mice were enriched for pathways associated with PDAC progression, including proliferation (*Cdk2/4*, *Ccnd2*, *E2f3*, *Bcl2*), angiogenesis (*Vegfa*, *Angpt2*, *Flt1*, *Pdgfa/b/c*, *Pdgfrb*, *Fgf9/18*), and ERK-associated signaling programs (*Tgfb1*, *Mif*, *Jun*, *Il1b*) (Fig. 8A,F). Also reduced were genes annotating to developmental and mesenchymal signaling pathways, including Wnt and Hedgehog signaling components (*Ctnnb1*, *Ihh*, *Smo*, *Sox9*), as well as genes involved in ECM remodeling and cancer-associated fibroblast activation (*Ccn2/Ct*gf, *Loxl2*, *Plod2*, *Mmp11*, *Fap*, *Fn1*, *Grem1*), and mediators of immunosuppressive tumor–stromal crosstalk (*Spp1*, *Cd44*, *Cxcr4*, *Mif*, *Twist1*, *Gpc1*). Notably, several genes suppressed by *C1qa* deletion (Fig. 8G) overlap with proteins associated with high C1q expression and poor survival in human PDAC (Fig. 2A)[24–29].

DISCUSSION

Prior work from our laboratory identified immune cell infiltration into skeletal muscle, muscle atrophy and fibrosis as defining features of PDAC cachexia in people[6] and mice[10], and implicated complement pathway activation as a contributing mechanism[5]. Here, we significantly extend these prior findings and identify complement component 1q (C1q), the initiating molecule of the classical complement cascade, as a required initiator of PDAC-induced muscle wasting and functional deficits, that may mediate these outcomes through coordinated effects in skeletal muscle, tumor, and systemic inflammatory compartments.

In skeletal muscle of both cachectic people and mice with PDAC, we found increased deposition of C1q and IgM, including areas of co-localization. IgM is a canonical activator of the classical complement pathway and upon engaging antigens or damage-associated neoepitopes it undergoes a conformational transition that enables C1q binding and initiates classical pathway activation[43]. IgM presents multiple C1q binding sites on a single molecule, making it a particularly potent initiator of complement activation[43]. The IgM-C1q colocalization in cachectic muscle therefore suggests classical complement activation, consistent with evidence that IgM deposition in skeletal muscle precedes downstream complement activation following ischemia-reperfusion injury[44].

Interestingly, although we found a ~40% overlap between C1q and IgM in skeletal muscle from cachectic mice and people with PDAC, this also means that ~60% of deposited C1q did not overlap with IgM, suggesting parallel IgM-independent roles of C1q. Some of this non-overlapping C1q may reflect binding to IgG, which is also deposited in cachectic PDAC muscle[45] and can engage C1q[43]. Unlike IgM, however, IgG is monomeric, and efficient C1q binding and activation through IgG requires clustering of multiple antigen-bound IgG molecules[43]. Beyond antibody-mediated engagement, C1q can directly bind to damage-associated neoepitopes exposed by apoptotic or necrotic myofibers, oxidized or ruptured membranes, or remodeling ECM, each of which have been demonstrated in the muscles from tumor-bearing hosts[46,47]. Whether such direct C1q binding activates classical complement depends on the abundance, clustering, and spatial distribution of C1q-binding ligands on the damaged surface, which determines whether sufficient multivalent engagement occurs to activate C1r and C1s. An alternative is complement-independent signaling whereby C1q acts as a ligand that can engage cellular receptors to regulate efferocytosis, immune cell polarization, and tissue remodeling, thereby influencing inflammation and repair even in the absence of complement activation. Regardless of the mechanism of C1q deposition in muscle, our findings that *C1qa* deletion is protective against KPC-induced immune cell infiltration, atrophy and fibrosis of muscle strongly suggests that C1q is not merely an inert bystander marker of muscle tissue damage but may contribute functionally to pathology.

In agreement with this role of C1q in skeletal muscle pathophysiology, recent work demonstrated that delivery of exogenous C1q to injured muscle promotes fibrosis and further established, in aged muscle, that C1q expression promotes the differentiation of fibroadipogenic progenitors (FAPs) and the development of fibrosis[18]. The authors further found that ex vivo treatment of FAPs with C1q increased the mRNA expression of several collagens and ECM remodeling factors, providing a mechanistic link between C1q and fibrosis. In close alignment with this, we show here that the KPC-induced increase in the mRNA levels of multiple collagens, ECM components and regulatory factors, and the associated development of fibrosis in WT mice are abolished in *C1qa*$^{-/-}$ KPC mice. Interestingly, others have shown that C1q mRNA

is upregulated in macrophages isolated from aged, acutely injured, and dystrophic muscle, and that C1r and C1s mRNA is increased in FAPs, compared to control muscle[17,18]. Although the current study was not set up to identify the cell-specific sources of C1 components in cachectic muscle, we have previously shown an expansion of FAPs and an increase in macrophages in skeletal muscle of cachectic mice and people with PDAC[6,10]. It is therefore possible that the increased C1q levels reported in skeletal muscle herein derive from macrophages. Similarly, it is also possible that the increased C1q levels in KPC tumors derive from tumor-associated macrophages (TAMs). Indeed, analysis of human PDAC single-cell RNA-sequencing data[35–37] demonstrated that C1q expression is predominantly localized to macrophages, consistent with prior reports identifying macrophages as a predominant source of secreted C1q in human PDAC tumors[48–50], and $C1q^+$ TAMs as among the most abundant immune populations in PDAC tumors[51–53]. We further reveal here that C1q protein expression in human PDAC tumors associates with poor survival and co-expresses with proteins associated with ECM remodeling, EMT, myeloid cell infiltration, cancer-associated fibroblasts, and tumor angiogenesis. This co-expression profile is consistent with recent findings that $C1q^+$ TAMs constitute an immunosuppressive population across multiple cancer types and that C1q signaling within the tumor microenvironment contributes to immune evasion and pathological stromal remodeling[20,54,55]. In alignment with those findings, KPC tumors from mice null for *C1qa* (i.e. host deletion of *C1qa*) showed suppressed gene expression programs linked to these pro-tumor pathways and an increased transcriptional program consistent with intratumoral cytotoxic immunity, including expansion of $CD8^+$ T cells and Granzyme B, which were confirmed histologically. Importantly, intratumoral $CD8^+$ T cell density and cytotoxic effector activity are among the strongest predictors of improved survival in PDAC[23,56], and $C1q^+$ macrophages have emerged as important mediators of their suppression across multiple solid tumor types, contributing to $CD8^+$ T cell dysfunction, impaired antitumor immunity, and resistance to immune checkpoint therapy[33,57–61]. That *C1qa* deletion simultaneously preserved skeletal muscle mass and fiber size and shifted the tumor immune landscape toward a less immunosuppressive, more cytotoxic state, raises the possibility that C1q sits at a convergence point between two major drivers of poor prognosis in PDAC, tumor immune evasion and cancer-induced muscle wasting.

Importantly, the KPC-induced increase in C1q in muscle and its role in the regulation of cancer-induced muscle atrophy extended beyond the diaphragm to muscles central to locomotion, including the tibialis anterior (TA) muscle. Indeed, *C1qa* mRNA, and C1q and IgM co-deposition were increased in the TA of KPC mice, and TA muscle mass and myofiber size were preserved in $C1qa^{-/-}$ KPC mice. Interestingly, our previously published data showed that, unlike in the diaphragm, there is no evidence of C3 or C5b-9 deposition in the TA of KPC mice, when measured via immunohistochemistry[5], suggesting that C1q may contribute to cancer-induced TA pathology through local mechanisms independent of detectable downstream complement activation and/or through indirect systemic effects. In support of the former, our transcriptomic analysis identified IL-1 signaling among the pathways selectively induced in muscle of WT, but not $C1qa^{-/-}$, KPC mice. In macrophages, C1q has been reported to modulate inflammasome-dependent IL-1 signaling independent of downstream complement activation[62,63]. Whether C1q similarly regulates this process in the context of PDAC-induced muscle inflammation remains to be determined but represents a plausible complement-independent mechanism linking C1q to local muscle pathology. In support of the latter, *C1qa* deletion significantly attenuated the KPC-induced increases in circulating CCL2 and Activin A. Interestingly CCL2, otherwise known as monocyte chemoattractant protein-1 (MCP-1), is increased in treatment naïve cachectic PDAC patients compared to weight stable PDAC patients[38], is sufficient to decrease grip strength and muscle fiber size[64], can recruit macrophages to tumors to promote cachexia[39], and can suppress appetite to cause cachexia[40]. It is therefore possible that inhibiting the increase in serum CCL2 levels in $C1qa^{-/-}$ mice plays a role in the observed protection against KPC-induced anorexia and cachexia. Similarly, Activin A levels are higher in cancer patients with cachexia than weight stable patients and correlate positively with weight loss[65], and Activin A is sufficient to induce muscle atrophy, body weight loss, weakness and the development of muscle fibrosis[66]. Here we found that the KPC-induced increase in serum Activin A levels in WT mice (~55 pg/ml) was significantly inhibited in $C1qa^{-/-}$ KPC mice (~25 pg/ml), although levels remained significantly elevated above non-cancer controls. Whether this difference between genotypes is sufficient to exert differential effects on cachexia-

associated biology is unknown. Collectively, these findings suggest that C1q may promote cancer cachexia through mechanisms extending beyond canonical complement activation within skeletal muscle, potentially by shaping the systemic inflammatory environment. Specifically, C1q appears to regulate circulating mediators linked to anorexia, muscle atrophy, and fibrotic remodeling, thereby implicating host-derived C1q as an upstream modulator of both local and systemic cachexia-driving pathways.

In summary, our findings here reveal that host-derived C1q is required for the pathological remodeling of skeletal muscle in response to KPC pancreatic tumors, and for driving pathological programs in the pancreatic tumor microenvironment, suggesting that C1q inhibition may represent a novel strategy to simultaneously maintain skeletal muscle health and dampen tumor immune evasion in PDAC. The patient impact of this could be improvements in physical function and overall survival, which are two key endpoints identified as central to regulatory approval for cancer cachexia[67,68]. In support of these key outcomes, our findings demonstrate that *C1qa* deletion preserves voluntary activity and grip strength in KPC tumor-bearing mice, and that high C1q expression in PDAC tumors (which our mouse data suggest derives from host cells) independently associates with poor survival in people. Consistent with these findings, increased classical complement pathway-related proteins in skeletal muscle are associated with greater declines across physical, functional, and patient-reported outcomes, including appendicular lean mass, peak oxygen consumption, and fatigue, in patients with prostate cancer[69]. We did not determine the impact of *C1qa* deletion on survival in orthotopic KPC mice, since survival in this model, unlike people with PDAC, is often heavily influenced by primary tumor size (which was not different between WT and *C1qa* mice) and associated local morbidity, including abdominal compression and impaired feeding. This represents a potential confounder when evaluating interventions targeting systemic manifestations such as cachexia. Indeed, improved survival in orthotopic murine models may primarily reflect reduced tumor size rather than direct modification of systemic disease mechanisms. Interestingly, an investigator-initiated phase I/II clinical trial is currently active at Roswell Park Comprehensive Cancer Center (NCT07214298) to evaluate pegcetacoplan, a small peptide inhibitor of complement C3, in combination with oxaliplatin, irinotecan, leucovorin, and fluorouracil (mFOLFIRINOX) in patients with metastatic PDAC. Although not a primary outcome measure, the trial includes an exploratory objective of determining whether complement blockade shifts innate and lymphocyte responses in the tumor toward a more productive antitumor immune response[70]. That objective directly parallels our experimental findings here that host-derived C1q suppresses intratumoral cytotoxic immunity, with *C1qa* deletion increasing $CD8^+$ T cell infiltration and Granzyme B expression in PDAC tumors in mice. However, as mentioned, pegcetacoplan acts at C3 which is the convergence point of the classical, lectin, and alternative pathways, whereas our data implicate C1q, an initiating component of the classical pathway that can also engage complement-independent signaling. It therefore remains to be determined whether C3 inhibition with pegcetacoplan is sufficient to recapitulate the full immunomodulatory and muscle-protective effects of C1q loss, or whether upstream C1-targeted strategies are required to capture C1q's full contributions. Although, to our knowledge, C1-targeting therapies have not been clinically tested in cancer patients, there are active trials and/or FDA approved therapies in other conditions. In this regard, Tanruprubart (ANX005), an anti-C1q monoclonal antibody which blocks C1q upstream of C1 complex assembly[71], is currently in Phase 3 clinical trials for Guillain-Barré syndrome, in which the complement system acts as a destructive driver of nerve damage; Sutimlimab, an anti-C1s monoclonal antibody that blocks classical pathway activation is FDA-approved for the treatment of cold agglutinin disease[72], a condition in which autoantibodies attach to red blood cells (RBCs) at colder temperatures, activating the classical complement pathway and leading to RBC hemolysis and; C1-esterase inhibitors, which suppress C1s and C1r activity through broader serine protease inhibition[73]. Together, these findings, along with evidence that C1s inhibition improves muscle health and attenuates fibrosis in preclinical models of acute injury, aging, and Duchenne muscular dystrophy[17,18], support C1 complex-targeting strategies as a potential therapeutic approach for muscle health that warrants further investigation in the context of cancer-induced muscle pathologies and cancer cachexia more broadly.

METHODS

Patient Samples

Patient demographics and clinicopathological data were collected from participants at diagnosis and are provided in Table S7. Rectus abdominis skeletal muscle biopsies were obtained from eligible patients following a prospective collection protocol approved by the Moffitt Cancer Center Scientific Review Committee and the University of Florida Institutional Review Board. All patients provided written informed consent prior to enrollment. The eligible population consisted of confirmed treatment-naïve PDAC patients undergoing surgical resection with curative intent at Moffitt Cancer Center between 2019 and 2024. Data from ten total patients was collected and analyzed, which included five cachectic and five weight-stable patients, with each group comprising three males and two females. Cachexia was defined as involuntary body weight loss of >5% during the 6 months preceding PDAC diagnosis[2]. Skeletal muscle biopsy portions were embedded in optimal cutting temperature (OCT) compound, frozen in liquid nitrogen–cooled isopentane and stored at −80°C until analysis.

Animals

The University of Florida Institutional Animal Care and Use Committee (IACUC) approved all animal procedures. Male 12–20-week-old C57BL/6J wild-type (WT; stock no. 000664) and C57BL/6J *C1qa*$^{-/-}$ mice (stock no. 031675) were purchased from The Jackson Laboratory (Bar Harbor, ME) and acclimatized for at least one week prior to experimentation. Animals were housed at 22 ± 2°C under a 14:10-h light/dark cycle with standard chow and water provided ad libitum.

Cancer Cachexia Model

Murine KPC FC1245 pancreatic cancer cells, isolated from the pancreatic tumor of an LSL-Kras$^{G12D/+}$; LSL-Trp53$^{R172H/+}$; Pdx-1-Cre mouse, were originally provided by Dr. David Tuveson (Cold Spring Harbor Laboratory, Cold Spring Harbor, NY). The authenticity of the KPC FC1245 cell line has been described previously[74]. Cell lines were verified to be mycoplasma-free prior to receipt and by IDEXX BioAnalytics using PCR evaluation. Cells were cultured in DMEM supplemented with 10% FBS and 1% penicillin/streptomycin at 37°C in 5% CO_2 and used at passage 10. To model human PDAC, age- and weight-matched C57BL/6J and *C1qa*$^{-/-}$ mice received orthotopic pancreatic injection of either 50 µL sterile saline (Sham) or 1.5x10^5 KPC cells in 50 µL saline (KPC). All mice received subcutaneous meloxicam (15 mg/kg) immediately before surgery and every 24 h for 72 h, and a single subcutaneous dose of Ethiqa-XR (3.25 mg/kg) before surgery.

Physiological and Behavioral Assessments

Body weight was recorded between 0900–1000 h on the day of injection, every 3 days until tumors were palpable (~6 days post-injection), and then daily thereafter. Food intake was recorded daily between 0900 and 1000 h, beginning once tumors were first palpable, and was calculated as the difference between chow provided and total chow remaining (including spilled material recovered from the bedding) for individually housed mice. Forelimb grip strength was measured using a BIO-GS4 grip strength meter (BIOSEB, North Pinellas Park, FL), with the peak value from three consecutive trials recorded per mouse. Spontaneous locomotor activity was recorded over a 24-hour light-dark cycle using a piezoelectric force-sensor actimetry platform (Activ Meter 2.0, BIOSEB; 1 cm resolution, 80 Hz sampling rate). Mice used for this were maintained under single-housing conditions throughout the study prior to transferring into individual monitoring cages. The first 24-hour light-dark cycle was excluded to allow acclimation to the novel cage environment, with activity recorded on the subsequent light-dark cycle corresponding to day 8-9 post-injection in Sham mice and day 12-13 in KPC tumor-bearing mice.

Tissue Harvest

Mice were euthanized 13 days post-inoculation when significant cachexia is observed in WT KPC mice, in our hands[10,75]. Skeletal muscles involved in locomotion (tibialis anterior, gastrocnemius, soleus), respiration (diaphragm), mastication (masseter), and deglutition (digastric), as well as heart, tumor, spleen, and gonadal fat, were collected and analyzed. Hindlimb muscles were harvested bilaterally, and their mass was

averaged. Tissues were either embedded in OCT for histology or flash-frozen in liquid nitrogen for molecular analyses and stored at −80°C until analysis.

Serum Cytokine Analysis

Blood was collected by terminal cardiac puncture from anaesthetized mice and allowed to clot at room temperature for 30 minutes. Samples were centrifuged at 2,000 g for 10 minutes at 4°C, and serum was collected, aliquoted, and stored at −80°C until analysis. Serum GDF-15 and Activin A were quantified by ELISA according to manufacturer instructions (GDF-15, R&D Systems #MGD150; Activin A, Life Technologies #EM3RB). Eighteen circulating cytokines, chemokines and growth factors were quantified by multiplex immunoassay using the Mouse High Sensitivity T-Cell 18-Plex Discovery Assay (MDHSTC18; Eve Technologies, Calgary, Alberta, Canada) on the Luminex 200 system (Luminex Corporation/DiaSorin) with Bio-Plex Manager software (Bio-Rad Laboratories). The 18-plex panel included GM-CSF, IFN-γ, IL-1α, IL-1β, IL-2, IL-4, IL-5, IL-6, IL-7, IL-10, IL-12(p70), IL-13, IL-17A, CXCL1/KC, CXCL5/LIX, CCL2/MCP-1, CXCL2/MIP-2, and TNF-α.

Immunofluorescence and Histological Analysis

OCT-embedded tissues were cryosectioned at 10 μm and mounted on positively charged glass slides. All primary antibody incubations were performed overnight at 4°C and all fluorescent secondary antibody incubations were performed for 1 h at room temperature, protected from light. Fluorescence imaging parameters were defined on secondary-only control sections processed in parallel. C1q deposition was assessed in human rectus abdominis sections using anti-C1q [7H8] (#ab11861, rat monoclonal, Abcam), in mouse diaphragm, tibialis anterior, KPC tumor sections using anti-C1q [4.8] (#ab182451, rabbit monoclonal, Abcam). C3 deposition in mouse diaphragm was assessed using FITC-conjugated anti-C3c (#ab4212, rabbit polyclonal, Abcam; raised against native full-length C3 protein). Spatial colocalization of C1q and its canonical ligand IgM was evaluated in human rectus abdominis and mouse diaphragm and tibialis anterior sections. Endogenous tissue-deposited IgM was detected using Alexa Fluor 594–conjugated goat anti-human IgM (heavy chain; #A21216, Invitrogen) for human muscle sections and Alexa Fluor 594–conjugated goat anti-mouse IgM (heavy chain; #A21044, Invitrogen) for mouse muscle sections. Myofiber cross-sectional area was quantified from WGA-stained sections in both human rectus abdominis and mouse TA, diaphragm, masseter, and digastric muscles using Alexa Fluor 594–conjugated WGA (#W11262, Invitrogen), as previously described[76,77]. Macrophages were quantified using anti-CD68 [FA-11] (#ab53444, rat monoclonal, Abcam). Neutrophils were quantified using anti-Ly6G (1A8, BioXcell). $CD8^+$ T cells were quantified using anti-CD8 (#98941, Cell Signaling Technology). Granzyme B expression was detected using anti-Granzyme B (#ab4059, Abcam). Nuclei were counterstained with DAPI (#D9542, Sigma-Aldrich). Masson's trichrome staining to detect collagen was performed on human rectus abdominis OCT-embedded cross-sections by the University of Florida Molecular Pathology Core facility, as previously described[6]. Picrosirius Red staining, where slides were fixed in Bouin's fluid and incubated for 90 min in picrosirius red solution (0.1% Direct Red 80 in saturated picric acid) prior to dehydration and cover slipping, was used to quantify collagen content in the diaphragm, and changes in the extracellular matrix were quantified by the percentage of the muscle area occupied by WGA-positive staining. Four non-overlapping images per section were captured on a Leica DM5000B microscope (×20 objective for immunofluorescence human rectus abdominis and mouse diaphragm, masseter, and digastric sections; ×10 objective for human rectus abdominis Masson's trichrome sections, mouse TA, and tumor sections). Myofiber cross-sectional area was quantified from WGA-stained images using Cellpose (v3.0, cyto3) and the LabelsToROIs ImageJ plugin, as previously described[78]. C1q, C3, and IgM were quantified by integrated density, with C1q-IgM colocalization assessed using Manders' coefficients, and $CD68^+$, $Ly6G^+$, and $CD8^+$ T cells counted manually. All measurements were performed on thresholded ImageJ images relative to secondary-only controls and normalized to the number of fields analyzed.

RNA Isolation, qRT-PCR, and Sequencing

Total RNA was isolated by TRIzol homogenization followed by chloroform phase separation and DNase treatment. RNA integrity was assessed using an Agilent TapeStation 4200 (Agilent Technologies). cDNA synthesis and qRT-PCR were performed using a QuantStudio 3 Real-Time PCR System (Applied Biosystems) with the following TaqMan probes (Thermo Fisher Scientific): *C1qa* (Mm07295529_m1) and *18S* (Hs03003631_g1). For library preparation and RNA sequencing, mouse TA and diaphragm samples were processed at Azenta Life Sciences, while tumor samples were processed at the University of Florida ICBR Gene Expression and Genotyping Core. Libraries were prepared from oligo(dT)-enriched mRNA using the NEBNext Ultra RNA Library Prep Kit for Illumina, validated on the TapeStation 4200, and quantified by Qubit 2.0 fluorometry and qPCR (KAPA Biosystems). Libraries were sequenced on an Illumina HiSeq 2000 (diaphragm and TA) or Illumina NovaSeq X Series (tumor) using a 2 × 150 bp paired-end configurations. Raw BCL files were converted to FASTQ and demultiplexed using bcl2fastq (v2.17). Reads were adapter-trimmed and aligned to the mouse GRCm38 reference genome using STAR (v2.5.2b). Gene-level counts were quantified with FeatureCounts. Differential expression analysis was performed using DESeq2 with Wald tests, and p-values were adjusted using the Benjamini–Hochberg false discovery rate correction (FDR q).

KPC RNA-seq Time Course Dataset

Diaphragm RNA-seq data from Sham and orthotopic KPC tumor-bearing mice across a time course of cachexia initiation and progression were extracted from our previously published dataset (GEO: GSE271521)[10].

PDAC Patient Datasets

Rectus abdominis muscle biopsy microarray data from PDAC patients (n = 20; 15 cachectic and 5 weight stable) were obtained from our previously published dataset (GEO: GSE130563)[6]. Microarray data were correlated with CT-derived skeletal muscle index and skeletal muscle attenuation values for these same patients that we previously published[30]. Primary tumor proteomic and clinical outcome data from 105 people in the Clinical Proteomic Tumor Analysis Consortium pancreatic ductal adenocarcinoma cohort (CPTAC-PDAC) were accessed using the cptac Python package (v0.9)[31]. Human PDAC single-cell RNA-sequencing data were analyzed through the Pancreas Precancer Atlas (https://www.pancreas-precancer-atlas.com/), which integrates published human PDAC tumor datasets[35–37].

Statistical Analysis

Data are presented as individual values with means ± SEM. Prior to parametric testing, data were assessed for normality using the Shapiro–Wilk test. Differences between two groups were assessed by unpaired two-tailed t-test or Mann-Whitney test; for more than two groups, one-way or two-way ANOVA with Tukey's HSD post hoc correction was used; correlations were analyzed by Pearson's correlation coefficient. Significance was defined as $p < 0.05$ unless otherwise specified. Circulating cytokine data were log-transformed to meet assumptions of normality and are presented on the linear scale. Differentially expressed genes (DEGs) were defined as $q < 0.05$ with log2FC > 1 (diaphragm), $q < 0.01$ with log2FC > 1 (tibialis anterior), or $q < 0.05$ with fold change > 1.2 (tumor), with tissue-specific thresholds reflecting differences in sample size, variability, and signal strength across datasets. DEGs were analyzed using DAVID (v2021) for Gene Ontology biological processes, KEGG pathways, and Reactome pathways. Enriched pathways were identified with an EASE score < 0.05. For CPTAC-PDAC survival analyses, of 137 patients with clinical annotation, 105 had matched proteomic data. After excluding patients with unknown resection status, n = 102 patients were stratified by median C1q subunit protein abundance (C1QA: 26.45, C1QB: 26.20, C1QC: 26.94 log2 relative intensity) for Kaplan–Meier analysis with log-rank comparison, and univariable Cox regression with C1q subunits modelled as continuous variables. Multivariable Cox models were adjusted for pathological stage, age, sex, and histologic grade (complete covariate data: n = 100; events per variable = 14.6), with proportional hazards verified by Schoenfeld residuals. CPTAC analyses were performed in Python 3.11 (lifelines v0.27); all other analyses were performed in GraphPad Prism (v10.2.3).

DATA AVAILABILITY

Raw sequencing data are publicly available as of the date of publication and have the following accession numbers, GEO: GSE337939 (diaphragm muscle), GEO: GSE338244 (tibialis anterior muscle), and GEO: GSE338245 (KPC pancreatic tumor).

REFERENCES

1. Baracos, V. E., Martin, L., Korc, M., Guttridge, D. C. & Fearon, K. C. H. Cancer-associated cachexia. *Nat Rev Dis Primers* **4**, 17105 (2018).
2. Fearon, K. *et al.* Definition and classification of cancer cachexia: an international consensus. *Lancet Oncol* **12**, 489–495 (2011).
3. Bachmann, J. *et al.* Cachexia Worsens Prognosis in Patients with Resectable Pancreatic Cancer. *Journal of Gastrointestinal Surgery* **12**, 1193–1201 (2008).
4. Nemer, L. *et al.* Predictors of Pancreatic Cancer–Associated Weight Loss and Nutritional Interventions. *Pancreas* **46**, 1152 (2017).
5. D'Lugos, A. C. *et al.* Complement pathway activation mediates pancreatic cancer-induced muscle wasting and pathological remodeling. *J Clin Invest* **135**, e178806 (2025).
6. Judge, S. M. *et al.* Skeletal Muscle Fibrosis in Pancreatic Cancer Patients with Respect to Survival. *JNCI Cancer Spectr* **2**, pky043 (2018).
7. Bhatt, B. J. *et al.* Molecular subtypes of human skeletal muscle in cancer cachexia. *Nature* **646**, 973–982 (2025).
8. Pryce, B. R. *et al.* Muscle inflammation is regulated by NF-κB from multiple cells to control distinct states of wasting in cancer cachexia. *Cell Rep* **43**, 114925 (2024).
9. Deyhle, M. R. *et al.* Depleting Ly6G Positive Myeloid Cells Reduces Pancreatic Cancer-Induced Skeletal Muscle Atrophy. *Cells* **11**, 1893 (2022).
10. Neyroud, D. *et al.* Local Inflammation Precedes Diaphragm Wasting and Fibrotic Remodelling in a Mouse Model of Pancreatic Cancer. *J Cachexia Sarcopenia Muscle* **16**, e13668 (2025).
11. Shukla, S. K. *et al.* Macrophages potentiate STAT3 signaling in skeletal muscles and regulate pancreatic cancer cachexia. *Cancer Lett* **484**, 29–39 (2020).
12. Chang, C.-J. *et al.* Macrophage activation determines muscle wasting in pancreatic cancer. *Oncogene* https://doi.org/10.1038/s41388-025-03434-9 (2025) doi:10.1038/s41388-025-03434-9.
13. Dunkelberger, J. R. & Song, W.-C. Complement and its role in innate and adaptive immune responses. *Cell Res* **20**, 34–50 (2010).
14. Mollnes, T. E., Song, W.-C. & Lambris, J. D. Complement in inflammatory tissue damage and disease. *Trends Immunol* **23**, 61–64 (2002).
15. Tsokos, G. C. & Fleming, S. D. Autoimmunity, Complement Activation, Tissue Injury and Reciprocal Effects. **7**, 149–164 (2003).
16. Nesargikar, P. N., Spiller, B. & Chavez, R. The complement system: history, pathways, cascade and inhibitors. *Eur J Microbiol Immunol (Bp)* **2**, 103–111 (2012).
17. Florio, F. *et al.* Combinatorial activation of the WNT-dependent fibrogenic program by distinct complement subunits in dystrophic muscle. *EMBO Molecular Medicine* **15**, e17405 (2023).
18. Kanugovi, A. *et al.* Targeting C1q signaling in fibro-adipogenic progenitors prevents regenerative fibrosis of aged muscle. *Proc Natl Acad Sci U S A* **123**, e2423340122 (2026).
19. Zhang, S. *et al.* C1q+ tumor-associated macrophages contribute to immunosuppression through fatty acid metabolic reprogramming in malignant pleural effusion. *J Immunother Cancer* **11**, e007441 (2023).
20. Bulla, R. *et al.* C1q acts in the tumour microenvironment as a cancer-promoting factor independently of complement activation. *Nat Commun* **7**, 10346 (2016).
21. Viiklepp, K. *et al.* Expression of C1q by Macrophages and Fibroblasts in Tumor Microenvironment Is Associated with Progression and Metastasis of Cutaneous Squamous Cell Carcinoma. *Journal of Investigative Dermatology* **145**, 2854-2868.e4 (2025).

22. Persky, J. *et al.* Characterization of natural killer and cytotoxic T-cell immune infiltrates in pancreatic ductal adenocarcinoma. *Journal of Surgical Oncology* **129**, 885–892 (2024).
23. Orhan, A. *et al.* The prognostic value of tumour-infiltrating lymphocytes in pancreatic cancer: a systematic review and meta-analysis. *European Journal of Cancer* **132**, 71–84 (2020).
24. Mascharak, S. *et al.* Desmoplastic stromal signatures predict patient outcomes in pancreatic ductal adenocarcinoma. *Cell Rep Med* **4**, 101248 (2023).
25. Alonso-Nocelo, M. *et al.* Macrophages direct cancer cells through a LOXL2-mediated metastatic cascade in pancreatic ductal adenocarcinoma. *Gut* **72**, 345–359 (2023).
26. Huang, Q., Liu, M. & Wu, W. Tumor-associated macrophages positive for SPP1 indicate a poorer clinical prognosis in pancreatic ductal adenocarcinoma. *Journal of Pancreatology* **8**, 279 (2025).
27. Wu, Y. *et al.* Integrative Single-Cell and Spatial Transcriptomics Analysis Reveals ECM-remodeling Cancer-associated Fibroblast-Derived POSTN as a Key Mediator in Pancreatic Ductal Adenocarcinoma Progression. *International Journal of Biological Sciences* **21**, 3573–3596 (2025).
28. Li, E., Cheung, H. C. (Zoey) & Ma, S. CTHRC1+ fibroblasts and SPP1+ macrophages synergistically contribute to pro-tumorigenic tumor microenvironment in pancreatic ductal adenocarcinoma. *Sci Rep* **14**, 17412 (2024).
29. Morin, E. *et al.* VEGF receptor-2/neuropilin 1 trans-complex formation between endothelial and tumor cells is an independent predictor of pancreatic cancer survival. *J Pathol* **246**, 311–322 (2018).
30. Judge, S. M. *et al.* MEF2c-dependent downregulation of Myocilin mediates cancer-induced muscle wasting and associates with cachexia in cancer patients. *Cancer Res* **80**, 1861–1874 (2020).
31. Cao, L. *et al.* Proteogenomic characterization of pancreatic ductal adenocarcinoma. *Cell* **184**, 5031-5052.e26 (2021).
32. Nosacka, R. L. *et al.* Distinct cachexia profiles in response to human pancreatic tumours in mouse limb and respiratory muscle. *J Cachexia Sarcopenia Muscle* **11**, 820–837 (2020).
33. Yi, F.-S. *et al.* Complement C1q is a key player in tumor-associated macrophage-mediated CD8+ T cell and NK cell dysfunction in malignant pleural effusion. *Int J Biol Sci* **20**, 5979–5998 (2024).
34. Mitchell, D. A. *et al.* C1q deficiency and autoimmunity: the effects of genetic background on disease expression. *J Immunol* **168**, 2538–2543 (2002).
35. Elhossiny, A. M. *et al.* Asynchronous Evolution of Epithelium and Stroma Differentiates Precursor Lesions from Pancreatic Cancer. *Cancer Discov* OF1–OF25 (2026) doi:10.1158/2159-8290.CD-25-2001.
36. Carpenter, E. S. *et al.* KRT17high/CXCL8+ Tumor Cells Display Both Classical and Basal Features and Regulate Myeloid Infiltration in the Pancreatic Cancer Microenvironment. *Clin Cancer Res* **30**, 2497–2513 (2024).
37. Steele, N. G. *et al.* Multimodal mapping of the tumor and peripheral blood immune landscape in human pancreatic cancer. *Nat Cancer* **1**, 1097–1112 (2020).
38. Talbert, E. E. *et al.* Circulating monocyte chemoattractant protein-1 (MCP-1) is associated with cachexia in treatment-naïve pancreatic cancer patients. *J Cachexia Sarcopenia Muscle* **9**, 358–368 (2018).
39. Liu, M. *et al.* The crosstalk between macrophages and cancer cells potentiates pancreatic cancer cachexia. *Cancer Cell* **42**, 885-903.e4 (2024).
40. Ibrahim, M. *et al.* Autophagy Suppresses CCL2 to Preserve Appetite and Prevent Lethal Cachexia. *bioRxiv* 2025.02.20.638910 (2025) doi:10.1101/2025.02.20.638910.
41. Zhong, X. *et al.* The systemic activin response to pancreatic cancer: implications for effective cancer cachexia therapy. *Journal of Cachexia, Sarcopenia and Muscle* **10**, 1083–1101 (2019).
42. Groarke, J. D. *et al.* Ponsegromab for the Treatment of Cancer Cachexia. *New England Journal of Medicine* **391**, 2291–2303 (2024).
43. Poon, P. H., Phillips, M. L. & Schumaker, V. N. Immunoglobulin M possesses two binding sites for complement subcomponent C1q, and soluble 1:1 and 2:1 complexes are formed in solution at reduced ionic strength. *Journal of Biological Chemistry* **260**, 9357–9365 (1985).

44. Chan, R. K. *et al.* IgM binding to injured tissue precedes complement activation during skeletal muscle ischemia-reperfusion. *Journal of Surgical Research* **122**, 29–35 (2004).
45. He, W. A. *et al.* NF-κB-mediated Pax7 dysregulation in the muscle microenvironment promotes cancer cachexia. *J Clin Invest* **123**, 4821–4835 (2013).
46. Thielens, N. M., Tedesco, F., Bohlson, S. S., Gaboriaud, C. & Tenner, A. J. C1q: A fresh look upon an old molecule. *Mol Immunol* **89**, 73–83 (2017).
47. Chen, Y., Park, Y.-B., Patel, E. & Silverman, G. J. IgM antibodies to apoptosis-associated determinants recruit C1q and enhance dendritic cell phagocytosis of apoptotic cells. *J Immunol* **182**, 6031–6043 (2009).
48. Kemp, S. B. *et al.* Pancreatic cancer is marked by complement-high blood monocytes and tumor-associated macrophages. *Life Science Alliance* **4**, (2021).
49. Steele, N. G. *et al.* Multimodal mapping of the tumor and peripheral blood immune landscape in human pancreatic cancer. *Nat Cancer* **1**, 1097–1112 (2020).
50. Revel, M., Sautès-Fridman, C., Fridman, W.-H. & Roumenina, L. T. C1q+ macrophages: passengers or drivers of cancer progression. *Trends in Cancer* **8**, 517–526 (2022).
51. Shakiba, M. & Tuveson, D. A. Macrophages and fibroblasts as regulators of the immune response in pancreatic cancer. *Nat Immunol* **26**, 678–691 (2025).
52. Liu, R., Li, J., Liu, L., Wang, W. & Jia, J. Tumor-associated macrophages (TAMs): Constructing an immunosuppressive microenvironment bridge for pancreatic ductal adenocarcinoma (PDAC). *Cancer Pathogenesis and Therapy* **3**, 183–196 (2025).
53. Yang, S., Liu, Q. & Liao, Q. Tumor-Associated Macrophages in Pancreatic Ductal Adenocarcinoma: Origin, Polarization, Function, and Reprogramming. *Front. Cell Dev. Biol.* **8**, (2021).
54. Kiecolt-Glaser, J. K. *et al.* Breast cancer survivors' typhoid vaccine responses: Chemotherapy, obesity, and fitness make a difference. *Brain, Behavior, and Immunity* **103**, 1–9 (2022).
55. Roumenina, L. T. *et al.* Tumor Cells Hijack Macrophage-Produced Complement C1q to Promote Tumor Growth. *Cancer Immunol Res* **7**, 1091–1105 (2019).
56. Liu, L. *et al.* Low intratumoral regulatory T cells and high peritumoral CD8+ T cells relate to long-term survival in patients with pancreatic ductal adenocarcinoma after pancreatectomy. *Cancer Immunol Immunother* **65**, 73–82 (2015).
57. Yang, Y. *et al.* The immune-metabolic crosstalk between CD3+C1q+TAM and CD8+T cells associated with relapse-free survival in HCC. *Front. Immunol.* **14**, (2023).
58. Li, Y. *et al.* Specific lineage transition of tumor-associated macrophages elicits immune evasion of ascitic tumor cells in gastric cancer with peritoneal metastasis. *Gastric Cancer* **27**, 519–538 (2024).
59. Dong, L. *et al.* The loss of RNA N6-adenosine methyltransferase Mettl14 in tumor-associated macrophages promotes CD8+ T cell dysfunction and tumor growth. *Cancer Cell* **39**, 945-957.e10 (2021).
60. Mezheyeuski, A. *et al.* An immune score reflecting pro- and anti-tumoural balance of tumour microenvironment has major prognostic impact and predicts immunotherapy response in solid cancers. *eBioMedicine* **88**, 104452 (2023).
61. Markiewski, M. M. *et al.* Modulation of the antitumor immune response by complement. *Nat Immunol* **9**, 1225–1235 (2008).
62. Benoit, M. E., Clarke, E. V., Morgado, P., Fraser, D. A. & Tenner, A. J. Complement Protein C1q Directs Macrophage Polarization and Limits Inflammasome Activity during the Uptake of Apoptotic Cells. *J Immunol* **188**, 5682–5693 (2012).
63. Wu, X.-Y. *et al.* Complement C1q synergizes with PTX3 in promoting NLRP3 inflammasome over-activation and pyroptosis in rheumatoid arthritis. *J Autoimmun* **106**, 102336 (2020).
64. Alissa, N. *et al.* CCL2 signaling promotes skeletal muscle wasting in non-tumor and breast tumor models. *Dis Model Mech* **17**, dmm050398 (2024).
65. Loumaye, A. *et al.* Role of Activin A and myostatin in human cancer cachexia. *J Clin Endocrinol Metab* **100**, 2030–2038 (2015).

66. Chen, J. L. *et al.* Elevated expression of activins promotes muscle wasting and cachexia. *FASEB J* **28**, 1711–1723 (2014).
67. Fioretti, F. *et al.* Cachexia and Wasting in Chronic Illness: Regulatory and Clinical Trial Update. *Journal of Cachexia, Sarcopenia and Muscle* **16**, e70128 (2025).
68. Dajani, O. *et al.* Oncological and Survival Endpoints in Cancer Cachexia Clinical Trials: Systematic Review 6 of the Cachexia Endpoints Series. *J Cachexia Sarcopenia Muscle* **16**, e13756 (2025).
69. Caeiro, L. *et al.* Muscle mitochondria, function, mass, and quality of life in prostate cancer during androgen deprivation therapy. *Nat Commun* **17**, 6884 (2026).
70. Roswell Park Cancer Institute. *A Phase I/II Study of Complement Inhibition in Pancreatic Ductal Adenocarcinoma*. https://clinicaltrials.gov/study/NCT07214298 (2026).
71. Kroon, H.-A. *et al.* Efficacy and Safety of Targeted Immunotherapy with ANX005 in Treating Guillain-Barré Syndrome: A Phase 3 Multicenter Study (PL5.006). *Neurology* **104**, 4954 (2025).
72. Röth, A. *et al.* Sutimlimab in Cold Agglutinin Disease. *New England Journal of Medicine* **384**, 1323–1334 (2021).
73. Defendi, F., Amen, A., Clavarino, G. & Dumestre-Pérard, C. C1 inhibitor: from complement system to bradykinin angioedema. *Current Opinion in Immunology* **97**, 102653 (2025).
74. Sivaram, N. *et al.* Tumor-intrinsic PIK3CA represses tumor immunogenecity in a model of pancreatic cancer. *J Clin Invest* **129**, 3264–3276 (2019).
75. Neyroud, D. *et al.* Blocking muscle wasting via deletion of the muscle-specific E3 ligase MuRF1 impedes pancreatic tumor growth. *Commun Biol* **6**, 519 (2023).
76. Duckett, S. M. *et al.* Murine pancreatic tumors induce pathological remodeling of muscles critical to chewing and swallowing. *American Journal of Physiology-Cell Physiology* https://doi.org/10.1152/ajpcell.00390.2026 (2026) doi:10.1152/ajpcell.00390.2026.
77. Ducharme, J. B. *et al.* Identification of a senescence-associated transcriptional program in skeletal muscle of cachectic pancreatic-tumor-bearing mice. *Am J Physiol Cell Physiol* **328**, C1125–C1134 (2025).
78. Ducharme, J. B. *et al.* Dietary supplementation with ursolic acid preserves skeletal muscle mass and strength in mouse models of cancer cachexia. *American Journal of Physiology-Cell Physiology* https://doi.org/10.1152/ajpcell.00159.2026 (2026) doi:10.1152/ajpcell.00159.2026.

AUTHOR CONTRIBUTIONS

JBD, CA, SMJ, and ARJ conceived and designed the study; JBD, MMS, BRP, NMA, SMD, RAV, TB, MAP, JBP, SMJ, and ARJ participated in data acquisition; JBD, MMS, BRP, CA, SMJ, and ARJ contributed to data analysis and interpretation; JBD and ARJ wrote the manuscript, which was then edited by DJD, CA, and SMJ. All authors read and approved the submitted version.

ACKNOWLEDGEMENTS

This work was supported by the National Institute of Arthritis and Musculoskeletal and Skin Diseases (R01AR060209 to ARJ, R01AR081648 to ARJ and CA [Multiple Principal Investigators]), the National Cancer Institute (NCI) (R01CA270025 to SMJ), and by the James and Esther King Biomedical Research Program, Florida Department of Health #24K03 to JBP and ARJ. JBD was supported by an NCI training grant (T32CA257923) and the UF Health Cancer Institute, which is supported in part by state appropriations provided in Florida Statute 381.915 and the NCI (P30CA247796).

DECLARATION OF INTERESTS

The authors declare no competing interests.

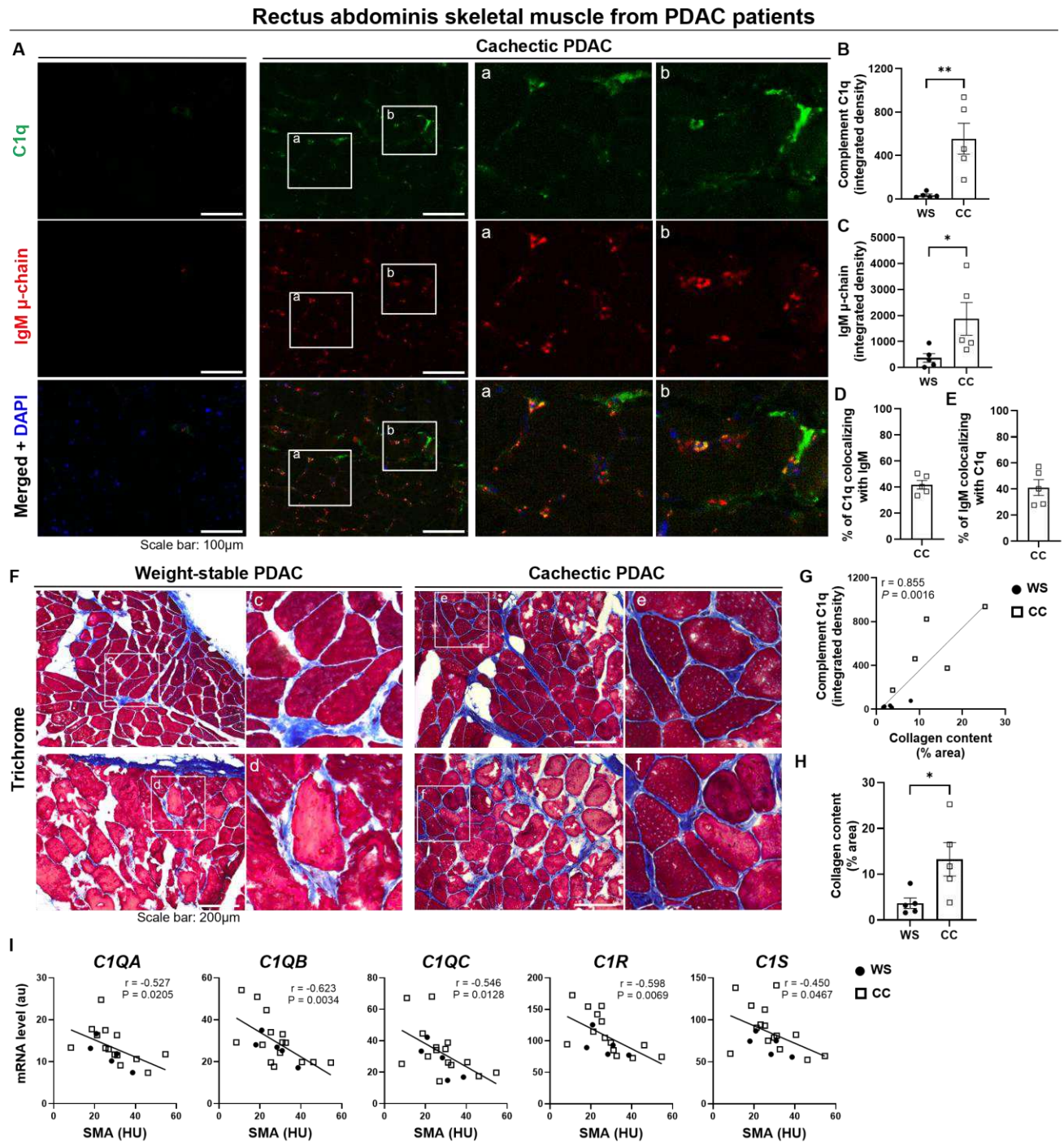

Rectus abdominis skeletal muscle from PDAC patients
A
Cachectic PDAC
C1q
IgM µ-chain
Merged + DAPI
Scale bar: 100µm
B
Complement C1q (integrated density)
WS
CC
C
IgM µ-chain (integrated density)
D
% of C1q colocalizing with IgM
E
% of IgM colocalizing with C1q
F
Weight-stable PDAC
Cachectic PDAC
Trichrome
Scale bar: 200µm
G
r = 0.855
P = 0.0016
Collagen content (% area)
H
I
C1QA
C1QB
C1QC
C1R
C1S
r = -0.527
P = 0.0205
r = -0.623
P = 0.0034
r = -0.546
P = 0.0128
r = -0.598
P = 0.0069
r = -0.450
P = 0.0467
mRNA level (au)
SMA (HU)

Figure 1. C1q is increased in skeletal muscle of cachectic PDAC patients and correlates with muscle fibrosis and reduced CT-derived muscle attenuation. Rectus abdominis muscle biopsies from weight-stable (WS; n = 5) and cachectic (CC; n = 5) PDAC patients, classified by international consensus criteria based on involuntary body weight loss of >5% during the 6 months preceding PDAC diagnosis. (A) Representative immunofluorescence for complement C1q (green) and IgM (a canonical ligand of C1q; red), merged with DAPI; insets (a, b) show high-magnification regions of colocalization. Scale bar, 100 μm. (B, C) Quantification of C1q and IgM integrated density. (D, E) Percentage of C1q colocalizing with IgM and vice versa. (F) Representative Masson's trichrome staining for collagen content; insets (c–f) show high-magnification regions. Scale bar, 200 μm. (G) Correlation between collagen content and C1q integrated density. (H) Quantification of collagen content (% area). (I) Correlation between CT-derived skeletal muscle attenuation (SMA, Hounsfield units) and rectus abdominis mRNA levels of *C1QA, C1QB, C1QC, C1R,* and *C1S* in a separate cohort of n = 20 PDAC patients (n = 15 CC, n = 5 WS). Data are mean ± SEM. *P < 0.05, **P < 0.01 by unpaired two-tailed Student's t-test or Mann-Whitney test (B, C, H) or Pearson correlation (G, I).

Tumor tissue from PDAC patients

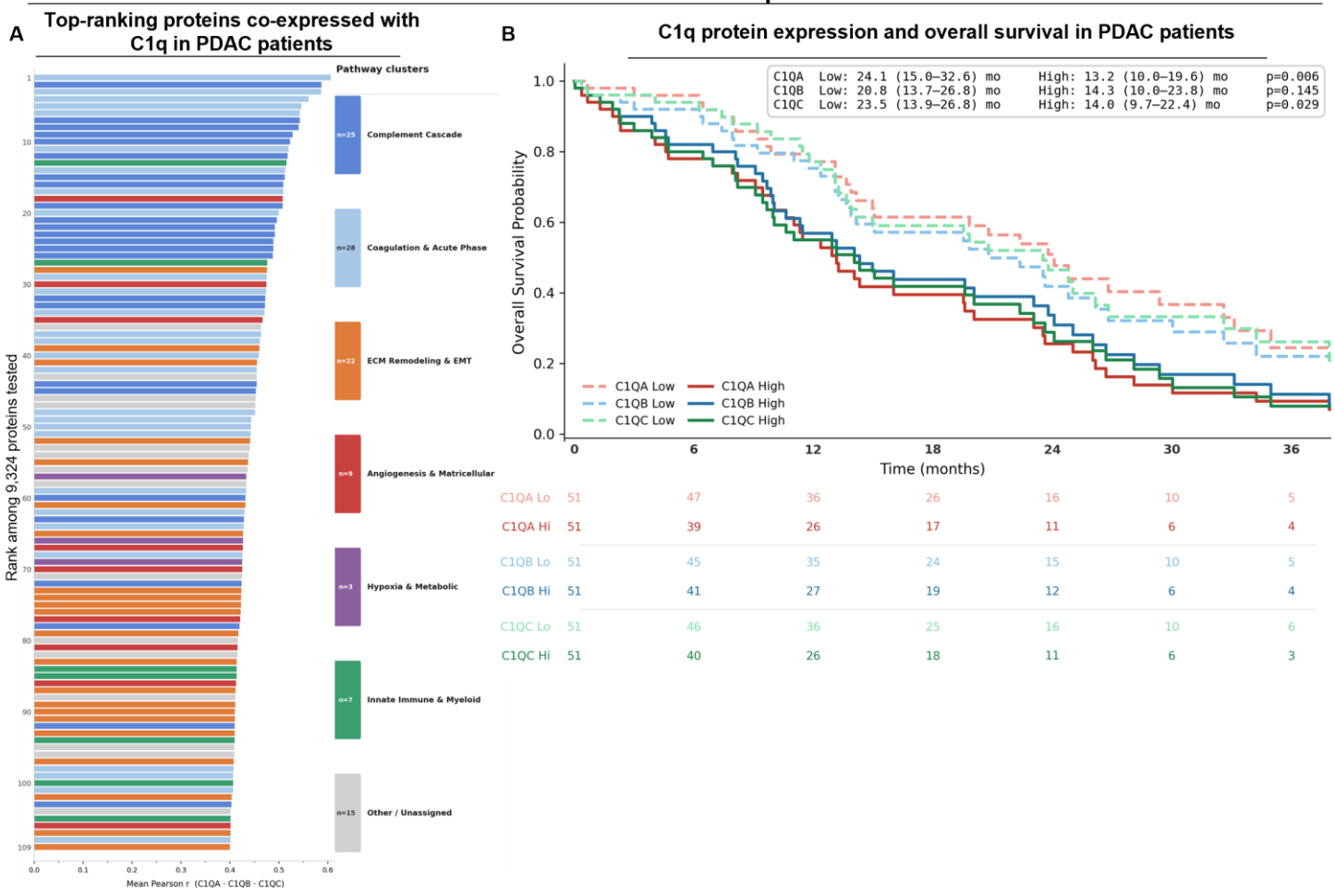


Figure 2. Tumor C1q protein expression correlates with complement pathways, immunosuppression programs and independently predicts poor survival in PDAC patients. (A) Top proteins co-expressed with C1q (mean Pearson r across C1QA, C1QB, C1QC; $r \geq 0.40$, $q < 0.05$) from a genome-wide screen of 9,324 proteins in PDAC tumor tissue from the Clinical Proteomic Tumor Analysis Consortium PDAC (CPTAC)-PDAC cohort (n = 105 people), annotated by pathway cluster; individual proteins are listed in Table S1. (B) Kaplan-Meier overall survival curves stratified by median-split tumor protein expression of C1QA, C1QB, and C1QC (n = 102 people). High C1QA expression was associated with reduced median survival (13.2 [95% CI 10.0–19.6] vs. 24.1 [15.0–32.6] months; log-rank P = 0.006), as was high C1QC expression (14.0 [9.7–22.4] vs. 23.5 [13.9–26.8] months; P = 0.029). C1QB showed a concordant but non-significant trend by median split (14.3 [10.0–23.8] vs. 20.8 [13.7–26.8] months; P = 0.145), reaching significance when modeled as a continuous variable in univariable Cox regression (Table S2). Numbers of patients at risk at each time point are shown below the plot.

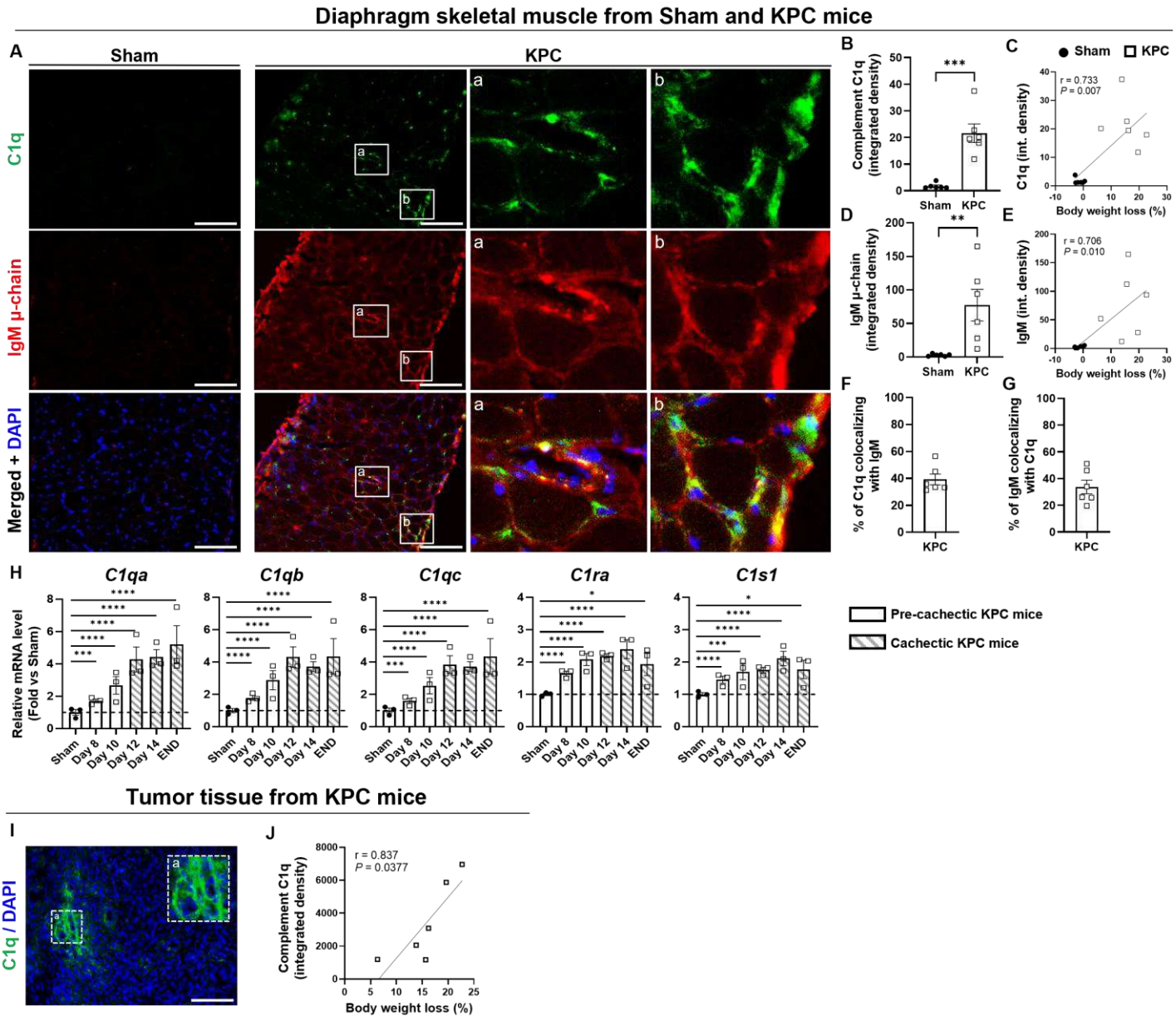

Diaphragm skeletal muscle from Sham and KPC mice
A
Sham
KPC
C1q
IgM µ-chain
Merged + DAPI
B
Complement C1q (integrated density)
***
Sham
KPC
C
Sham
KPC
r = 0.733
P = 0.007
C1q (int. density)
Body weight loss (%)
D
IgM µ-chain (integrated density)
**
Sham
KPC
E
r = 0.706
P = 0.010
IgM (int. density)
Body weight loss (%)
F
% of C1q colocalizing with IgM
KPC
G
% of IgM colocalizing with C1q
KPC
H
C1qa
C1qb
C1qc
C1ra
C1s1
Relative mRNA level (Fold vs Sham)
Sham
Day 8
Day 10
Day 12
Day 14
END
Pre-cachectic KPC mice
Cachectic KPC mice
Tumor tissue from KPC mice
I
C1q / DAPI
J
r = 0.837
P = 0.0377
Complement C1q (integrated density)
Body weight loss (%)

Figure 3. C1q accumulates in diaphragm and tumor of cachectic KPC mice and is associated with cachexia severity. (A) Representative immunofluorescence for C1q (green) and IgM (red) in diaphragm of Sham and KPC mice, merged with DAPI; insets (a, b) show high-magnification regions of colocalization. Scale bar, 100 μm. (B, D) Quantification of C1q and IgM integrated density. (C, E) Correlation of C1q and IgM integrated density with percentage body weight loss. (F, G) Percentage of C1q colocalizing with IgM and vice versa. (H) Relative diaphragm mRNA levels of *C1qa, C1qb, C1qc, C1ra,* and *C1s1* across the cachexia continuum (pre-cachectic: Day 8, 10; cachectic: Day 12, 14, End) relative to Sham, extracted from our previously published diaphragm RNA-seq time course (GEO: GSE271521). (I) Representative immunofluorescence for C1q (green) in KPC tumor tissue; inset (a) shows high-magnification region. Scale bar, 100 μm. (J) Correlation between tumor C1q integrated density and percent body weight loss. Data are mean ± SEM; n = 3-6 per group. *P < 0.05, **P < 0.01, ***P < 0.001, ****P < 0.0001 by unpaired two-tailed Student's t-test or Mann-Whitney test (B, D), one-way ANOVA with Tukey's HSD post hoc test vs. Sham (H), or Pearson correlation (C, E, J).

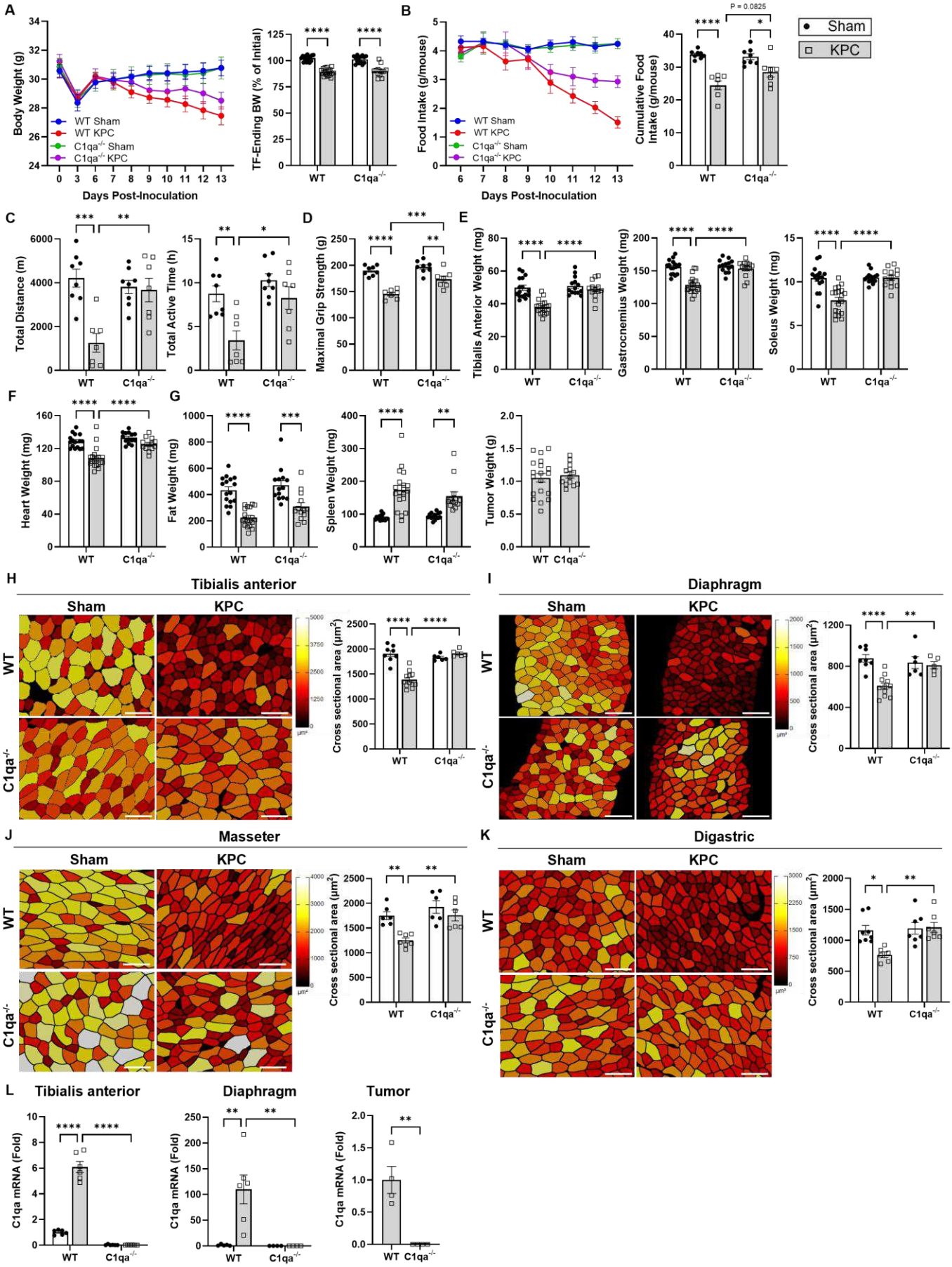

A
Body Weight (g)
WT Sham
WT KPC
C1qa-/- Sham
C1qa-/- KPC
Days Post-Inoculation
TF-Ending BW (% of Initial)
WT
C1qa-/-
B
Food Intake (g/mouse)
Days Post-Inoculation
Cumulative Food Intake (g/mouse)
P = 0.0825
Sham
KPC
C
Total Distance (m)
Total Active Time (h)
D
Maximal Grip Strength (g)
E
Tibialis Anterior Weight (mg)
Gastrocnemius Weight (mg)
Soleus Weight (mg)
F
Heart Weight (mg)
G
Fat Weight (mg)
Spleen Weight (mg)
Tumor Weight (g)
H
Tibialis anterior
Sham
KPC
WT
C1qa-/-
Cross sectional area (μm2)
I
Diaphragm
J
Masseter
K
Digastric
L
Tibialis anterior
Diaphragm
Tumor
C1qa mRNA (Fold)

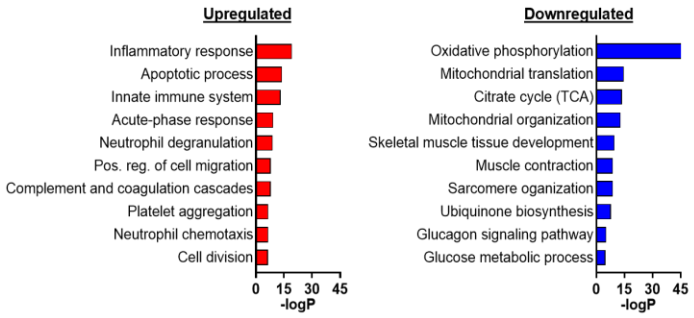
Figure 4. Genetic deletion of *C1qa* protects against KPC tumor-induced cachexia, muscle wasting, and functional decline. WT and *C1qa*$^{-/-}$ mice received orthotopic injection of saline (Sham) or KPC pancreatic cancer cells (KPC). (A) Body weight over time and tumor-free (TF)-ending body weight (% of initial). (B) Food intake over time and cumulative food intake. (C) Voluntary cage activity - total distance covered and active time in a 24 h period. (D) Maximal grip strength. (E) Tibialis anterior, gastrocnemius, and soleus muscle weights. (F) Heart weight. (G) Fat, spleen, and tumor weights. (H–K) Representative pseudo-colored cross-sectional area (CSA) images and quantification of mean myofiber CSA in tibialis anterior, diaphragm, masseter, and digastric muscles. Scale bar, 100 μm. (L) *C1qa* mRNA levels in tibialis anterior, diaphragm, and tumor determined by qRT-PCR. Data are mean ± SEM; n = 4-19 per group. *P < 0.05, **P < 0.01, ***P < 0.001, ****P < 0.0001 by two-way ANOVA with Tukey's HSD post hoc test (A-K, L; tibialis anterior and diaphragm) or unpaired two-tailed Student's t-test (L; tumor).

A

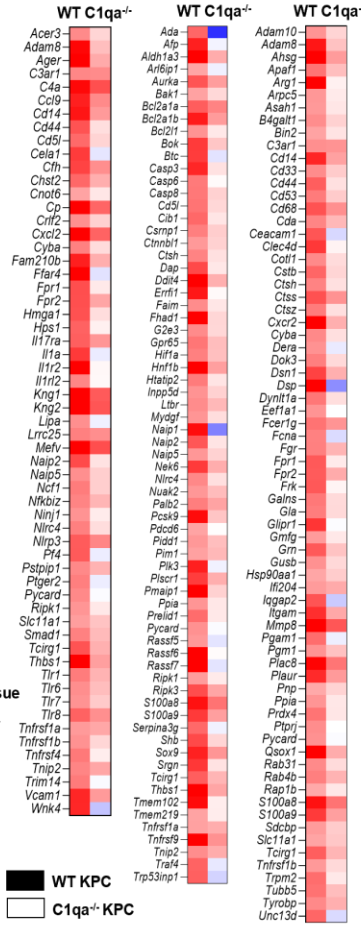
Diaphragm DEGs: FDR q < 0.05, Fold change > 2

	Total # Genes	# Upregulated	# Downregulated
WT, KPC vs Sham	3,291	1,786	1,503
C1qa$^{-/-}$, KPC vs Sham	955	456	499
DEGs only in WT	2,799	1,463	1,336

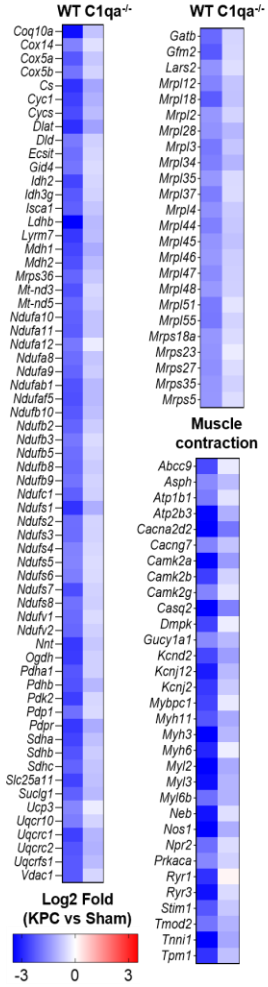
B



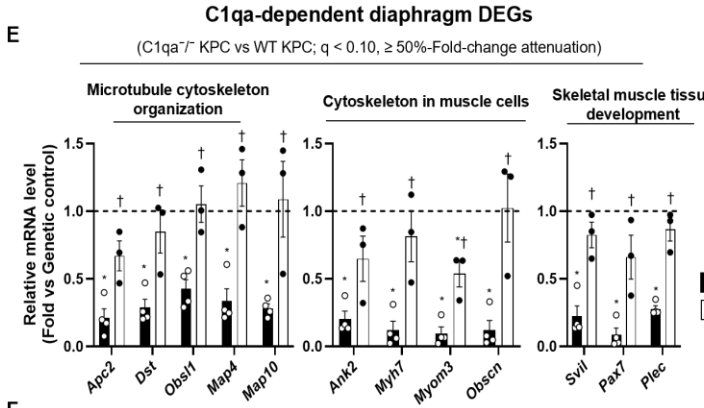
C Upregulated only in WT KPC



D Downregulated only in WT KPC



E



F

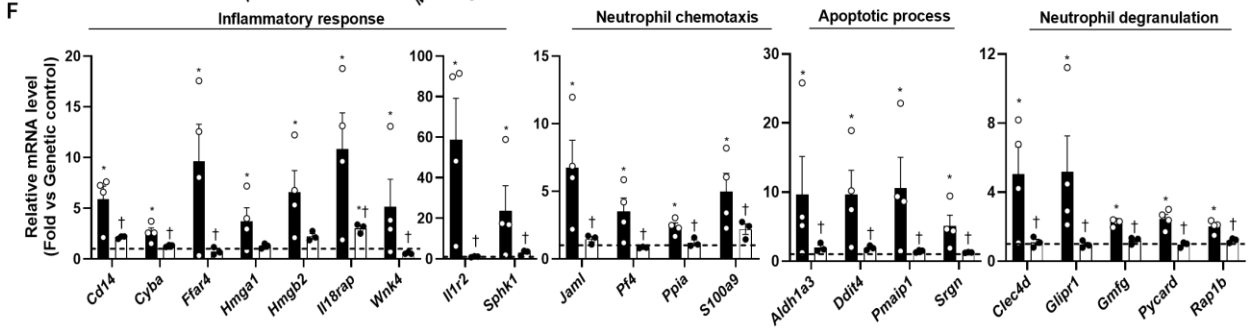


Figure 5. *C1qa* deletion attenuates inflammatory transcriptional programs while normalizing oxidative metabolic gene programs in diaphragms of mice with pancreatic cancer. RNA-seq of diaphragms from WT and *C1qa*$^{-/-}$ Sham and KPC mice. (A) Number of total, upregulated, and downregulated DEGs ($q < 0.05$, fold change > 2) for KPC vs. Sham in each genotype, and DEGs significant only in WT, but not *C1qa*$^{-/-}$, KPC mice. (B) Pathway enrichment of DEGs only in WT KPC. (C, D) Heatmaps of genes within significantly upregulated and downregulated pathways in WT, but not *C1qa*$^{-/-}$, KPC mice. (E-F) *C1qa*-dependent DEGs downregulated (E) and upregulated (F) by KPC tumors in WT mice and rescued by *C1qa* deletion ($q < 0.10$, ≥50% fold-change attenuation). Data in E, F are mean ± SEM relative to genetic control (dotted line); n = 3-4 per group. *$P < 0.05$ vs. genotype-matched Sham; †$P < 0.05$ vs. WT KPC.

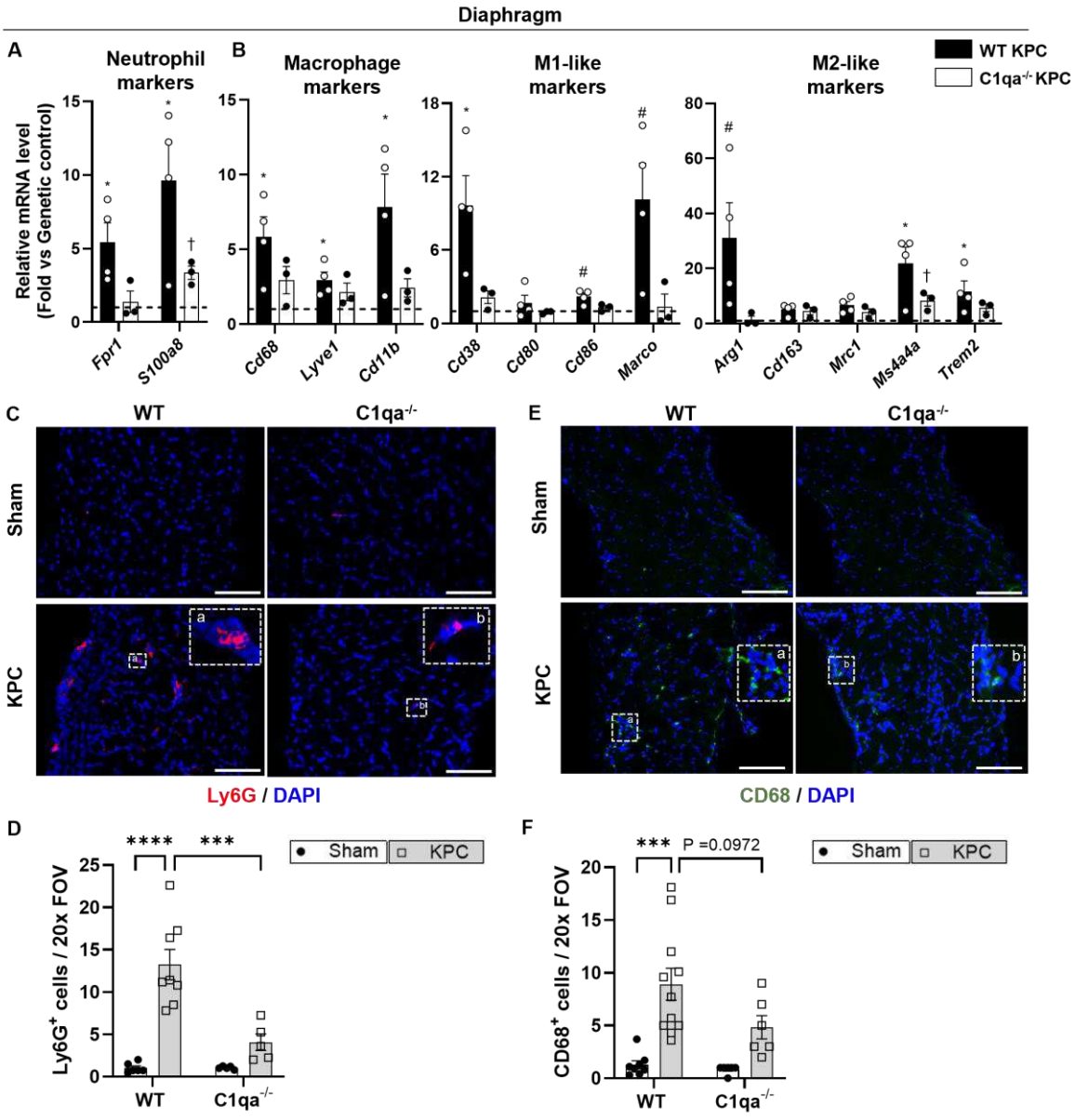

Diaphragm
A
Neutrophil markers
B
Macrophage markers
M1-like markers
M2-like markers
WT KPC
C1qa-/- KPC
Relative mRNA level (Fold vs Genetic control)
Fpr1
S100a8
Cd68
Lyve1
Cd11b
Cd38
Cd80
Cd86
Marco
Arg1
Cd163
Mrc1
Ms4a4a
Trem2
C
WT
C1qa-/-
Sham
KPC
Ly6G / DAPI
E
CD68 / DAPI
D
Ly6G+ cells / 20x FOV
****
***
Sham
KPC
F
CD68+ cells / 20x FOV
*** P =0.0972

Figure 6. *C1qa* deletion inhibits KPC-induced leukocyte trafficking into the diaphragm. (A, B) Relative diaphragm mRNA levels of neutrophil markers, macrophage markers (including resident marker *Lyve1* and recruited marker *Cd11b*), M1-like markers, and M2-like markers in WT and *C1qa*$^{-/-}$ KPC mice, extracted from bulk diaphragm RNA-seq and normalized to genotype-matched Sham (dotted line). (C) Representative Ly6G (red)/DAPI immunofluorescence in diaphragm of WT and *C1qa*$^{-/-}$ Sham and KPC mice. (D) Quantification of Ly6G^{+} neutrophils per 20× field of view (FOV). (E) Representative CD68 (green)/DAPI immunofluorescence. (F) Quantification of CD68^{+} macrophages per 20× FOV. Data are mean ± SEM; n = 3-12 per group. *P < 0.05 vs. genotype-matched Sham; †P < 0.05, #P < 0.10 vs. WT KPC (A, B); ***P < 0.001, ****P < 0.0001 (D, F) by two-way ANOVA with Tukey's HSD post hoc test.

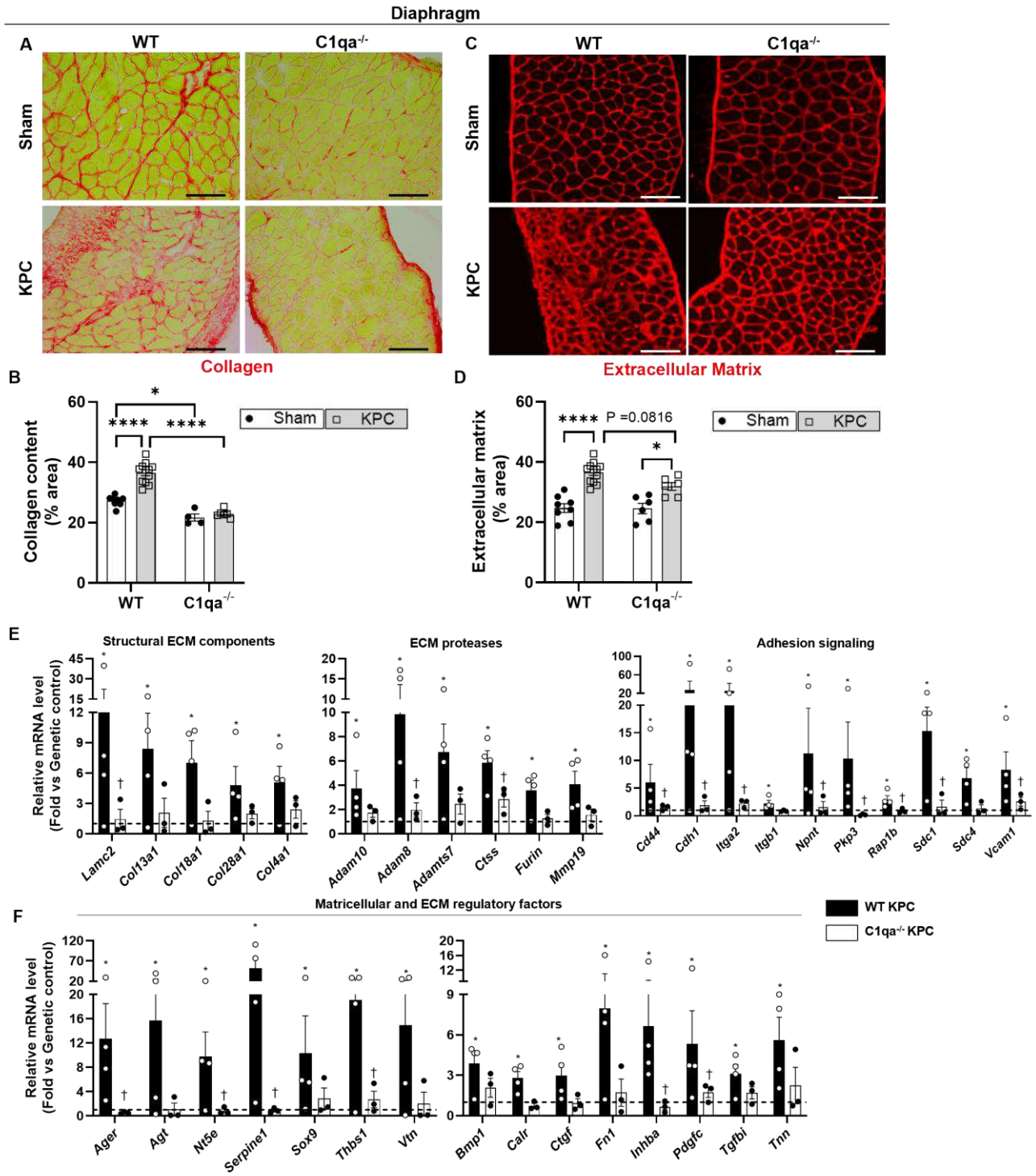

Diaphragm
A
WT
C1qa-/-
Sham
KPC
Collagen
C
Extracellular Matrix
B
Collagen content (% area)
Sham
KPC
WT
C1qa-/-
D
Extracellular matrix (% area)
P =0.0816
E
Structural ECM components
Relative mRNA level (Fold vs Genetic control)
Lamc2
Col13a1
Col18a1
Col28a1
Col4a1
ECM proteases
Adam10
Adam8
Adamts7
Ctss
Furin
Mmp19
Adhesion signaling
Cd44
Cdh1
Itga2
Itgb1
Npnt
Pkp3
Rap1b
Sdc1
Sdc4
Vcam1
F
Matricellular and ECM regulatory factors
WT KPC
C1qa-/- KPC
Ager
Agt
Nt5e
Serpine1
Sox9
Thbs1
Vtn
Bmp1
Calr
Ctgf
Fn1
Inhba
Pdgfc
Tgfbi
Tnn

Figure 7. *C1qa* deletion prevents KPC-induced collagen deposition and attenuates extracellular matrix expansion and remodeling gene expression in the diaphragm. (A) Representative picrosirius red staining for collagen in diaphragm of WT and *C1qa*$^{-/-}$ Sham and KPC mice. (B) Quantification of collagen content (% area). (C) Representative wheat germ agglutinin (WGA) staining of the extracellular matrix (ECM). (D) Quantification of ECM content (% area). (E-F) Relative mRNA levels, extracted from bulk diaphragm RNA-seq, of structural ECM components, ECM proteases, adhesion signaling genes, and matricellular and ECM regulatory factors normalized to genotype-matched Sham (dotted line). Data are mean ± SEM; n = 3-12 per group. *P < 0.05, ****P < 0.0001 (B, D); *P < 0.05 vs. genotype-matched Sham, †P < 0.05 vs. WT KPC (E,F), by two-way ANOVA with Tukey's HSD post hoc test

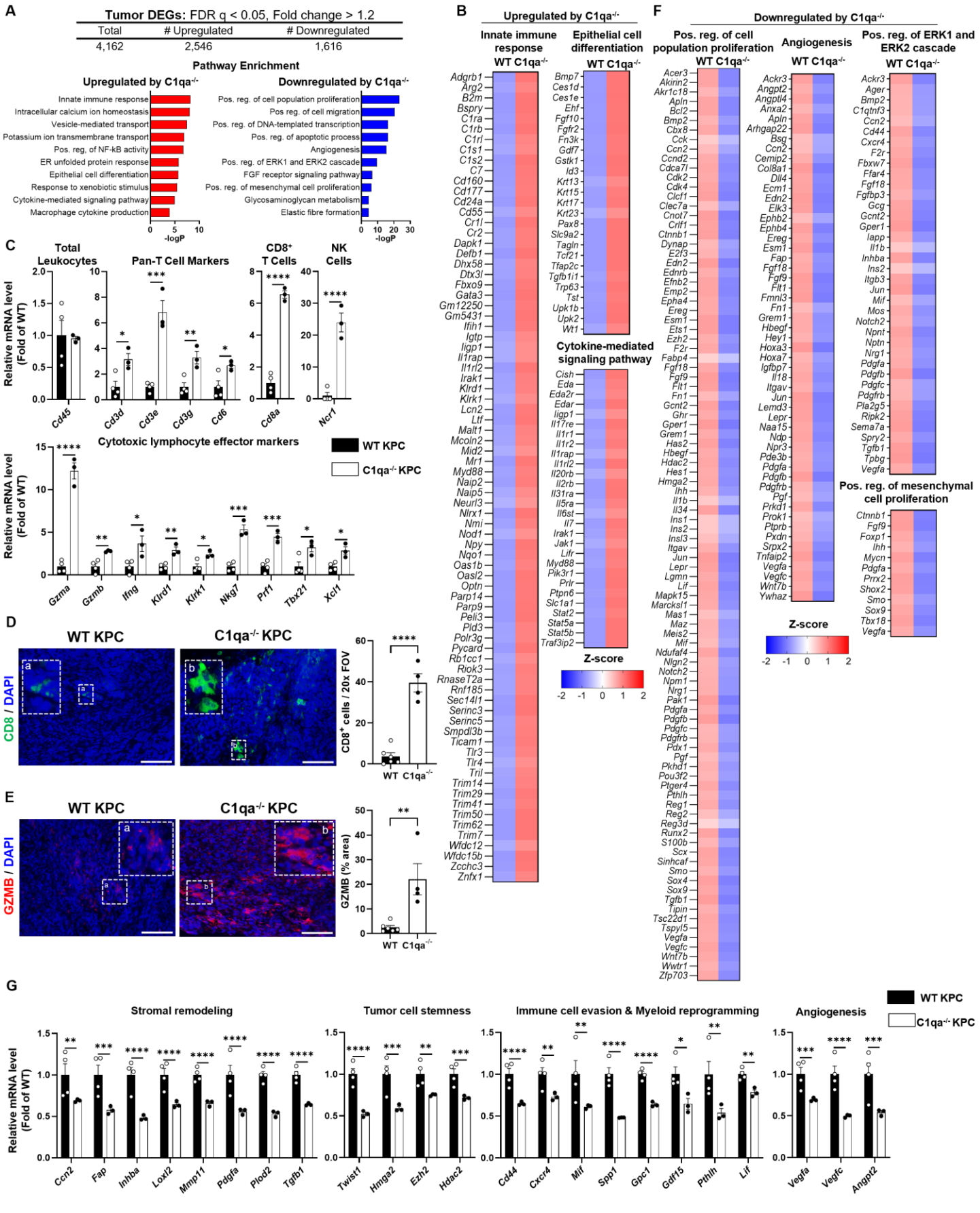

A
Tumor DEGs: FDR q < 0.05, Fold change > 1.2
Total
Upregulated
Downregulated
4,162
2,546
1,616
Pathway Enrichment
Upregulated by C1qa-/-
Innate immune response
Intracellular calcium ion homeostasis
Vesicle-mediated transport
Potassium ion transmembrane transport
Pos. reg. of NF-kB activity
ER unfolded protein response
Epithelial cell differentiation
Response to xenobiotic stimulus
Cytokine-mediated signaling pathway
Macrophage cytokine production
-logP
Downregulated by C1qa-/-
Pos. reg. of cell population proliferation
Pos reg. of cell migration
Pos. reg. of DNA-templated transcription
Pos. reg. of apoptotic process
Angiogenesis
Pos. reg. of ERK1 and ERK2 cascade
FGF receptor signaling pathway
Pos. reg. of mesenchymal cell proliferation
Glycosaminoglycan metabolism
Elastic fibre formation
-logP
B
Upregulated by C1qa-/-
Innate immune response
WT C1qa-/-
Epithelial cell differentiation
WT C1qa-/-
Cytokine-mediated signaling pathway
Z-score
F
Downregulated by C1qa-/-
Pos. reg. of cell population proliferation
WT C1qa-/-
Angiogenesis
WT C1qa-/-
Pos. reg. of ERK1 and ERK2 cascade
WT C1qa-/-
Pos. reg. of mesenchymal cell proliferation
Z-score
C
Total Leukocytes
Pan-T Cell Markers
CD8+ T Cells
NK Cells
Relative mRNA level (Fold of WT)
Cd45
Cd3d
Cd3e
Cd3g
Cd6
Cd8a
Ncr1
Cytotoxic lymphocyte effector markers
WT KPC
C1qa-/- KPC
Gzma
Gzmb
Ifng
Klrd1
Klrk1
Nkg7
Prf1
Tbx21
Xcl1
D
WT KPC
C1qa-/- KPC
CD8 / DAPI
CD8+ cells / 20x FOV
WT
C1qa-/-
E
WT KPC
C1qa-/- KPC
GZMB / DAPI
GZMB (% area)
WT
C1qa-/-
G
WT KPC
C1qa-/- KPC
Stromal remodeling
Ccn2
Fap
Inhba
Loxl2
Mmp11
Pdgfa
Plod2
Tgfb1
Tumor cell stemness
Twist1
Hmga2
Ezh2
Hdac2
Immune cell evasion & Myeloid reprogramming
Cd44
Cxcr4
Mif
Spp1
Gpc1
Gdf15
Pthlh
Lif
Angiogenesis
Vegfa
Vegfc
Angpt2
Relative mRNA level (Fold of WT)

Figure 8. *C1qa* deletion reprograms the tumor immune microenvironment toward a cytotoxic lymphocyte signature while suppressing pro-tumorigenic stromal, proliferative, and angiogenic programs. RNA-seq of KPC tumors from WT and *C1qa*$^{-/-}$ mice. (A) Number of total, upregulated, and downregulated DEGs ($q < 0.05$, fold change > 1.2) and pathway enrichment for genes up- or downregulated by *C1qa* deletion. (B) Heatmaps of genes within significantly upregulated pathways. (C) Relative mRNA levels of total leukocyte, pan-T cell, CD8$^+$ T cell, NK cell, and cytotoxic lymphocyte effector markers in WT and *C1qa*$^{-/-}$ KPC tumors extracted from KPC tumor bulk RNA-seq. (D) Representative CD8 (green) and DAPI immunofluorescence and quantification of CD8$^+$ cells per 20× FOV; insets (a, b) show high-magnification regions. (E) Representative Granzyme B/GZMB (red) and DAPI immunofluorescence and quantification of GZMB$^+$ area; insets (a, b) show high-magnification regions. (F) Heatmaps of genes within significantly downregulated pathways. (G) Relative mRNA levels of genes involved in stromal remodeling, tumor cell stemness, immune evasion/myeloid reprogramming, and angiogenesis decreased by *C1qa* deletion extracted from bulk RNA-seq; several of these genes overlap with proteins associated with high tumor C1q expression and poor survival in human PDAC (Fig. 2A). Data are mean ± SEM; n = 4-6 per group. *$P < 0.05$, **$P < 0.01$, ***$P < 0.001$, ****$P < 0.0001$ by unpaired two-tailed Student's t-test or Mann-Whitney test.

Supplementary Files

This is a list of supplementary files associated with this preprint. Click to download.

- TableS1.xlsx
- TableS4.xlsx
- TableS3.xlsx
- SupportingInformation.docx
- TableS6.xlsx